



Paleostress evolution of the West Africa passive margin: New insights from calcite twinning paleopiezometry in the deeply buried syn-rift TOCA formation (Lower Congo basin)

Boubacar Bah^{a,*}, Olivier Lacombe^a, Nicolas E. Beaudoin^b, Aniès Zeboudj^a, Claude Gout^{b,c}, Jean-Pierre Girard^{b,c}, Pierre-Alexandre Teboul^c

^a Sorbonne Université, Institut des Sciences de la Terre de Paris (ISTeP), CNRS-INSU, Paris 75005, France

^b Université de Pau et des Pays de l'Adour, Laboratoire des Fluides Complexes et Leurs Réservoirs (LFCR), E2S UPPA, CNRS, TotalEnergies, Pau 64000, France

^c TotalEnergies, Centre Scientifique et Technique Jean Féger (CSTJF), Pau 64000, France.

ARTICLE INFO

Keywords:

Calcite twins
Paleostress
Tectonic stress
Paleopiezometry
Passive margin

ABSTRACT

Accurate characterization of hydrocarbon reservoirs requires a good understanding of the paleostress history of their host sedimentary basin. This study aims at reconstructing the paleoburial and paleostress history of the syn-rift Barremian TOCA Fm. in the Lower Congo basin (West African margin). Two oriented borehole cores drilled offshore Congo were investigated using stress inversion techniques applied to calcite mechanical twins to constrain paleostress orientations and magnitudes. The inversion of calcite twins was performed on a widespread early diagenetic cement (~129 to ~113 Ma) and revealed that the TOCA Fm. has undergone a complex poly-phase stress history, including (1) extensional stress regimes with vertical σ_1 and horizontal σ_3 trending NE-SW and WNW-ESE (N100) associated with the rifting episode preceding the opening of the South Atlantic (130 to 112 Ma), and with mean differential stresses of ~47 MPa for (σ_1 - σ_3) and ~20 MPa for (σ_2 - σ_3). The early N100 extension is associated with the development of normal faults striking N-S that likely reactivated inherited basement structures. The direction of extension evolved during the Barremian into the main NE-SW extension marked by the dominant normal faults striking NW-SE. (2) Compressional and strike-slip stress regimes with horizontal σ_1 oriented ~N-S possibly related to the far-field intraplate transmission of orogenic stresses generated at the distant Africa-Eurasia plate boundary at ~67–60 Ma, and with mean differential stresses of 40 MPa for (σ_1 - σ_3) and 28 MPa for (σ_2 - σ_3). (3) Compressional and strike-slip stress regimes with horizontal σ_1 oriented ENE-WSW to ~E-W that we tentatively relate to the mid-Atlantic ridge push and prevailing since ~15 Ma onwards, associated with mean differential stresses of ~45 MPa for (σ_1 - σ_3) and ~18 MPa for (σ_2 - σ_3). Our results reveal that the TOCA Fm. recorded mainly far-field stress effects that could be related to interactions between the African plate and surrounding plates, and that divergent passive margins may experience a complex tectonic history including both extensional and compressional events.

1. Introduction

Continental rifting and drifting result in the formation of divergent passive margins. During the rifting stage, extensional stress generally prevails. This extensional stress originates from boundary tectonic forces linked to plate motions, to frictional forces exerted by the convective mantle at the base of the lithosphere (e.g., Ziegler et al., 1995), and, to a lesser extent to body forces developing in the lithosphere above mantle plumes (Bott, 1993; Burov and Gerya, 2014;

Koptev et al., 2018). Structural and thermo-rheological inheritance may also play a role in modulating the local response of the rifted lithosphere (Cloetingh et al., 2013), causing high levels of structural complexity and possibly changing regional or local trends of extension during rifting (Morley et al., 2007).

The present-day stress pattern in the lithosphere is controlled at first order by plate boundary forces (Heidbach et al., 2007). At the regional scale, however, additional local sources of stress are necessary to fully account for the orientation of the horizontal maximum principal stress

* Corresponding author.

E-mail address: boubacar.bah@sorbonne-universite.fr (B. Bah).

<https://doi.org/10.1016/j.tecto.2023.229997>

Received 21 December 2022; Received in revised form 20 July 2023; Accepted 25 July 2023

Available online 26 July 2023

0040-1951/© 2023 Elsevier B.V. All rights reserved.

S_H and the tectonic regime. Within the oceanic part of plates, the oceanic ridge push often governs the intraplate stress field. This statement is supported by the observation that, in many instances, the intraplate S_H trends perpendicular to oceanic ridges in a strike-slip or thrust faulting regime (Zoback, 1992; Heidbach et al., 2008, 2016). At passive margins, the present-day stress field is often dominated by a S_H oriented roughly perpendicular to both the trend of the margin and the oceanic ridge and in a strike-slip or thrust faulting regime, so the ridge push is thought to be a possible significant source of the present-day stress at passive margins (e.g., Pascal and Cloetingh, 2009). Other stress sources, such as gravitational stress arising from (1) lithosphere bending due to loading related to rapid sedimentation rates, (2) postglacial rebound, and (3) difference in elevation and associated gravitational potential energy between the continent and the margin, should not be neglected (Pascal, 2006; Pascal and Cloetingh, 2009). However, those are often considered as being of local and/or short term importance (Seeber and Armbruster, 1988; Stein et al., 1989; Zoback, 1992). During the long lasting post-rift evolution of passive margins between continental break-up to present day, it is also likely that both ridge push and far-field compressional tectonic stresses transferred from distant convergent plate boundaries may have, at least transiently, played some role (Ziegler et al., 1995; Withjack et al., 1995; Vagnes et al., 1998).

The South Atlantic passive margins result from the rifting between Africa and South America and subsequent oceanization (e.g., Chaboureaud et al., 2013). However, their evolution is currently a matter of debate (Karl et al., 2013), with two contrasting theories on the tectonic and paleostress evolution on both sides of the South Atlantic (Salomon et al., 2015). Some authors argue that the Brazilian and SW African margins were influenced by flexure due to offshore sediment loading (e.g., Lima et al., 1997; Dauteuil et al., 2013; Reis et al., 2013). Cobbold et al. (2001) argue that the distant stresses of the Andean orogeny caused compression perpendicular to the Brazilian continental margin throughout the Cenozoic. On the African margin the upwelling of the African superplume, a large thermal anomaly in the lower mantle beneath southern Africa (e.g., Ritsema et al., 2011), is thought to be responsible for the high mean topography of southern and eastern Africa (e.g., Al-Hajri et al., 2009; Moucha and Forte, 2011; Flament et al., 2014).). The model of Japsen et al. (2012) favours the idea that both continental margins underwent the same multiple uplift events driven by the transfer of far-field stresses from one continent to the other. The different interpretations summarized above illustrate that the stress evolution at divergent passive margins like the West Africa margin is still poorly understood. Consequently, a better appraisal of the behaviour of divergent continental margins before and after continental break-up is essential to the understanding of plate tectonics and of the respective contribution of far-field gravitational or tectonic stresses. However, our knowledge of the paleostress history of passive margins suffers from the lack of direct paleostress information gained directly in the offshore domain.

Recent discoveries of deeply buried hydrocarbon reservoirs offshore Brazil have renewed the interest in understanding the sedimentary, burial and structural evolution of the presalt sedimentary series (Davison, 2007; Carminatti et al., 2008; Saller et al., 2016; see synthesis in Teboul, 2017). The term “pre-salt” refers to the lower Cretaceous deposits (mainly carbonates) underlying the widespread upper Aptian salt deposits (Guardado et al., 1989; McHargue, 1990; Dale et al., 1992). Structural and stratigraphic similarities of the plays encountered in both the Brazilian and the West African conjugate margins have been thoroughly documented (Brownfield and Charpentier, 2006; Chaboureaud et al., 2013; Péron-Pinvidic et al., 2017; Thompson et al., 2015), inducing a similar exploration scheme for both areas. In subsurface exploration, structural information comes mainly from seismic data, while stratigraphic, sedimentary and burial information comes from the study of drilling cores in exploration wells (Bjørlykke, 2014). In offshore sedimentary environments, especially in carbonate series, mesoscale fractures and stylolites as well as deformation microstructures such as

calcite twins observed at core scale are the main markers of deformation and the main fingerprints of the stress evolution (Beaudoin and Lacombe, 2018). The analysis of calcite twins is a long established tool to unravel the paleostress history (see review in Lacombe, 2010 and Lacombe et al., 2021a), allowing for the reconstruction of both paleostress orientations and magnitudes in a variety of settings, including sedimentary basins (Lacombe et al., 1990; Lacombe et al., 1994; Rocher et al., 2000, 2004; Kulikowski and Amrouch, 2017), fold-and-thrust belts (Craddock et al., 1993; Rocher et al., 1996; Lacombe, 2001; Lacombe et al., 2007, 2009; Amrouch et al., 2010, 2011) and even oceanic environments (Craddock and Pearson, 1994, Craddock et al., 2004; Brandstätter et al., 2017).

This study aims at reconstructing the paleostress history of the deeply buried, Barremian (130–125 Ma) TOCA Fm. (TOCA stands for TOp CARbonates) in the offshore Lower Congo basin (West Africa passive margin) using the inversion of calcite mechanical twins for stress from two oriented deep borehole cores. The TOCA Fm. was selected because it is a syn-rift unit (Harris, 2000; Beglinger et al., 2012) and is therefore likely to have recorded most of the tectonic evolution of the South Atlantic since the early Cretaceous. In order to depict the most complete paleostress history of the Lower Congo Basin, our stress results will be combined with the results of recent studies on the burial and diagenetic history of the TOCA Fm. (Bah et al., 2023) and on the burial and stress evolution of the post-rift Sendji Fm. (Zeboudj et al., 2023).

Our study therefore complements earlier paleostress studies conducted onshore West Africa in the Inkisi group (Paleozoic sandstone) in Republic of Congo (Nkodia et al., 2020), in the Etendeka volcanics and the Twyfelfontein Sandstone (Neocomian-Barremian) in Namibia (Salomon et al., 2015) and in the Proterozoic metamorphic rocks in Namaqualand, western South Africa (Viola et al., 2012). It must be noticed that because syn-rift formations are often scarce or absent onshore, the dating of the paleostress events has only been indirect to date, i.e., based mainly on regional correlations of paleostress orientations. Beyond providing important information on the timing and nature of the paleostress regimes at the reservoir scale, this study will also feed the debate about the extent to which far-field tectonic and gravitational lithospheric stress transferred from active plate boundaries may have played a role in the evolution of the West African passive margin. To that respect, the work reported here has implications for the interpretation of the dynamics of divergent passive margins worldwide.

2. Geological setting

2.1. Tectono-sedimentary framework of the West Africa margin

The south Atlantic continental margins are the result of Jurassic to Cretaceous rifting and subsequent continental breakup between the South American and African plates during the dislocation of the megac-continent Gondwana (Mohriak et al., 2008; Matton and Jébrak, 2009; Pletsch et al., 2001; Szatmari and Milani, 2016). Different rift segments were generated under an overall NE-SW-oriented extension during the opening of the South Atlantic (Rabinowitz and LaBrecque, 1979; Moulin et al., 2010; Chaboureaud et al., 2013): the equatorial segment, the central segment, the southern segment and the Falkland segment, the central segment being the focus of this study. These segments are characterized by distinct extensional and subsidence histories and are bounded by NE-SW-striking transform structures (Mbina Mounquengui and Guiraud, 2009).

The West African central segment is composed of three main sedimentary basins, namely: the Gabon, Lower Congo and Kwanza basins (Fig. 1a) (Standlee et al., 1992). These basins are characterized by the presence of a salt layer approximately 1 to 2 km thick (Brognon and Verrier, 1966; Masson, 1972; Brice et al., 1982; Giresse, 1982; Teisserenc and Villemin, 1989), overlying mainly continental sedimentary sequences (145–116 Ma). The salt is overlain by marine clastics and carbonates (112 Ma to present day) (Doyle et al., 1982; Mussard, 1996).

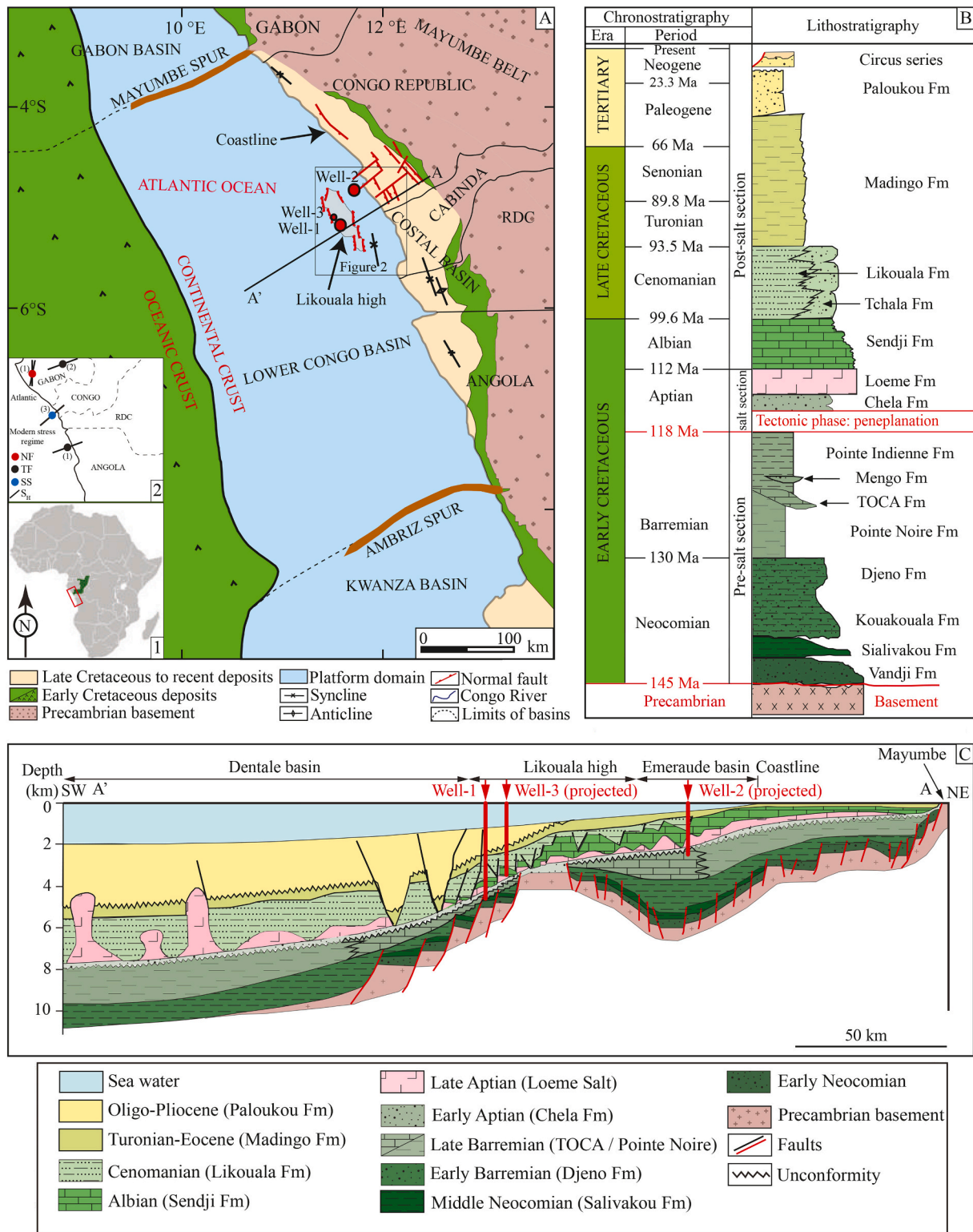


Fig. 1. (A) Structural map of Africa along the South Atlantic from Gabon to Angola with basins location. Modified after Zeboudj et al., 2023. In the marine domain, the Cretaceous oceanic crust is represented by the green colour. The insert (1) shows the location of the study area. The insert (2) shows the present-day stress regime derived from earthquake focal mechanism (1) from Nkodia et al. (2022) and (2) from Heidbach et al. (2016), respectively, and from borehole breakouts (3) (unpublished TotalEnergies report). (B) Stratigraphic chart of Lower Congo basin modified from unpublished TotalEnergies internal report. (C) Regional geological cross-section through the Congolese margin. Modified after Vernet et al., 1996 (see 1A for section location). (For interpretation of the references to colour in this figure legend, the reader is referred to the web version of this article.)

Three tectono-sedimentary episodes have marked the history of the central segment: continental rifting, transition phase (or rift/drift - sag cycle) and post-rift (or post-salt/drift - marginal sag) episodes (Da Costa et al., 1999; Karner et al., 2003; Contrucci et al., 2004; Moulin et al., 2005; Aslanian et al., 2009; Beglinger et al., 2012; Chaboureaud et al., 2013).

The first part of the rift phase (Neocomian to middle Barremian) is characterized by extensional tectonic activity that produced a series of horsts and grabens (Lehner and De Ruiter, 1977; Karner et al., 1997; Contrucci et al., 2004; Beglinger et al., 2012). These faulted blocks developing from the Atlantic hinge towards the mainland have allowed the sedimentation of two *syn*-rift sequences that correspond to lacustrine series with black clays laterally passing to sandstones and conglomerates on the rift margin (Karner et al., 1997; Marton et al., 2000; Séranne and Anka, 2005; Brownfield and Charpentier, 2006). The sandstone-conglomerate series consists of the Basal Sandstone and includes formations with names that change according to the different segments of the margin: Vandji - Lucula - Basal Sandstone - N'dombo (Fig. 1b). Tectonic activity decreased from the middle Barremian to the early Aptian, with draping of the tilted blocks and clay bevels on the high zones. This decrease or even stop of tectonic activity either would announce the sag period (Beglinger et al., 2012), or corresponds to a third *syn*-rift phase characterized by a sealing series of shallow lacustrine sandstone-clays (Contrucci et al., 2004; Séranne and Anka, 2005).

The Aptian transition phase marks the transition between rifting and thermally-induced lithospheric subsidence affecting the South Atlantic basins. This phase corresponds to the end of crustal stretching, rifting and basement faulting activity (Uncini et al., 1998; Beglinger et al., 2012), and is marked by the 'break-up unconformity' (Beglinger et al., 2012) along with evaporite deposition (Lehner and De Ruiter, 1977; Teisserenc and Villemin, 1989; Aslanian et al., 2009). The phase started with deposition of a transgressive clastic sequence, fluvio-deltaic sandstone and lacustrine clays, which evolved upwards into evaporite alternations. Subsequently, these series were sealed by widespread salt deposition during the middle and late Aptian (Burwood, 1999; Séranne and Anka, 2005). The onset of salt deposition is probably linked to progressive marine transgressions in the proto-South Atlantic (Asmus and Ponte, 1973; Beglinger et al., 2012) and to more arid conditions (Bate, 1999; Karner and Gambôa, 2007).

The post-rift phase started in the Albian times and is marked by continental break-up and subsequent oceanization (Aslanian et al., 2009; Guiraud et al., 2010). The post-rift phase is characterized by thermal subsidence, regional marine transgression to the north and gravity-driven salt tectonics (Lehner and De Ruiter, 1977; Guiraud and Maurin, 1991; Dingle, 1999; Karner and Driscoll, 1999). The series deposited during this stage can be divided into 3 sedimentary episodes. The first episode (Albian to Eocene) is characterized by a long-term retrograding sedimentary system in which marine carbonate sediments were deposited on top of the previous evaporitic series on a ramp/platform in a shallow marine environment (Beglinger et al., 2012). From the late Turonian onwards, the depositional environments changed drastically, with progressive disappearance of carbonates and deposition of shallow to deep clastics (Beglinger et al., 2012). Consequently, a new ramp profile of the margin developed. The end of this episode, from the Senonian to the early Paleogene, is marked by a drastic decrease in the sedimentation rate (Séranne and Anka, 2005). From the lower Oligocene onwards, a major stratigraphic reorganization prevailed in the Southwest African margin. After a phase of submarine erosion linked to sea level fall, a prograding sedimentary system developed from the Miocene to the present day probably linked to the onset of a deltaic system and to the proper thermal subsidence of the passive margin which continued after the transition phase (Contrucci et al., 2004). Finally, the prograding sedimentary system extended towards the deep basin generating the vast turbidite system of the deep Congo fan, while sedimentation continued on the platform with fine terrigenous or hemipelagic inputs reworked by deep-sea currents (Séranne and Anka,

2005).

2.2. Paleostress history and contemporary stress of the South-West Africa passive margin

The South Atlantic margins underwent a complex tectonic and paleostress history owing to their geodynamic evolution. This section summarizes published data on the past and present stress states of the West African margin in the South Atlantic. Stress orientations reported hereinafter refer to the current African plate position.

The Inkisi Group (early to middle Paleozoic: pre-late Carboniferous) is one of the red beds units that crop out in the Congo basin and are observed also in boreholes inside the Congo basin (Delvaux et al., 2021). Within the Congo basin, they are covered by the Late Carboniferous-Permian Lukuga series (belonging to the Karoo Supergroup) which are locally deformed as seen in the Dekese well and also in seismic profiles (Daly et al., 1992; Kadima et al., 2011; Delvaux et al., 2021). Late Jurassic-Cretaceous sedimentary series lie unconformably on the Inkisi Group. During the pre-rift phase, the Congo basin therefore recorded a major deformation phase sometimes between the Permian and the Jurassic that has been related to the Gondwanides orogeny on the southern margin of the Gondwana (Johnston, 2000).

During the rifting phase (late Jurassic to early Cretaceous), the West African margin underwent a NE-SW extension linked to the opening of the Atlantic Ocean (Rabinowitz and LaBrecque, 1979; Nurnberg and Müller, 1991). In Namibia, Salomon et al. (2015) highlighted two extensional trends: (1) an ENE-WSW extension perpendicular to the continental margin and related to continental rifting and (2) a NNE-SSW extension the importance of which remains unclear. Viola et al. (2012) also identified a ENE-WSW extension further south in South Africa.

During the post-rift phase, the western coast of South Africa underwent a major uplift from the Albian to the Turonian (115–90 Ma) (Kounov et al., 2009). This uplift triggered an erosion of up to 2–3 km and has been related to an E-W extensional event (Viola et al., 2012). In the Lower Congo basin, Zeboudj et al. (2023) reported extensional stress regimes with σ_3 trending ~N-S and ~E-W associated with thin-skinned salt tectonics that prevailed between ca 101 and 80 Ma in the offshore domain. Two distinct phases of N-S to NW-SE intraplate compression and a NE-SW extension were also identified (Viola et al., 2012). These stress regimes were not dated but were tentatively correlated, mainly on the basis of consistent stress orientations, to the compressional (and extensional) tectonic events recognized in Central and North Africa by Guiraud and Bosworth (1997), namely (1) late Santonian N-S to NW-SE compression; (2) Campanian-Maastrichtian NE-SW extension; (3) late Maastrichtian N-S to NW-SE compression. These compressional events are related to a plate reorganization during the Alpine cycle and to the shift in the opening directions of the Atlantic oceanic spreading centers and the subsequent counter clockwise rotational northward drift of Africa-Arabia into Eurasia. A strike-slip stress regime associated with a horizontal principal stress σ_1 oriented NW-SE has also been documented in continental Congo (Nkodia et al., 2020) and in Namibia (Salomon et al., 2015). Although still not precisely dated because of the lack of stratigraphic constraints, this stress regime was tentatively related to the late Santonian NW-SE compression of Guiraud and Bosworth (1997) and/or to the NNW-SSE compressional phase of Viola et al. (2012). In the Lower Congo basin, Zeboudj et al. (2023) reported post-75 Ma strike-slip stress regimes with σ_1 trending ~NW-SE to NNE-SSW and a compressional stress regime with σ_1 trending NNW-SSE that were attributed to the late Maastrichtian (–early Paleocene) compression of Guiraud and Bosworth (1997).

At the present day, an ENE-WSW to E-W oriented compression has been identified on both margins of the South Atlantic ocean, in Central Africa (Ziegler et al., 1995; Delvaux and Barth, 2010; Heibach et al., 2016) and in Brazil (Fernandes and Amaral, 2002; Salomon et al., 2015). In the segment of the margin investigated in this study, the few available stress data indicate a S_H oriented nearly perpendicular to both the

passive continental margin and the mid-Atlantic ridge, in Gabon (World Stress Map, S_H oriented N70 - N70 stands for N070°E hereinafter -, compressional stress regime) and in offshore Republic of Congo (borehole breakout data from petroleum wells, unpublished TotalEnergies report, S_H oriented N50, strike-slip stress regime) (Fig. 1a). The recent inversion of earthquake focal mechanisms (Nkodia et al., 2022) reveals a compressional stress regime with S_H oriented N70 in offshore Angola in the Lower Congo basin that progressively switches to a strike-slip stress regime with S_H oriented N80 to N100–120 (ENE-WSW to WNW- ESE) in the interior of the Congo basin. Along the West African margin in Gabon, these authors also document a contemporary extensional stress regime with S_H oriented N-S to NNE-SSW while the stress regime is compressional with a S_H oriented ~N80 in the interior Gabon.

On the basis of the analysis of mesoscale faults in the Inkisi Group in onshore Congo, Nkodia et al. (2020) identified a strike-slip stress regime with σ_1 oriented N70 which trend is close to the ENE-WSW S_H trend of the current state of stress (insert 2 of Fig. 1A). In the absence of any time constraint, the authors speculate that this stress regime would have started in the Miocene and would be related to some degree to the Atlantic ridge push. A strike-slip stress regime and a compressional stress regime with σ_1 trending ~E-W were recognized in the post-rift section in the Lower Congo basin by Zeboudj et al. (2023); these stress regimes likely prevailed from 15 Ma onwards and were also interpreted as originated from the Atlantic ridge push. The changes in the late Tertiary/contemporary stress regime (S_H ~ ENE-WSW in either reverse or strike-slip fault regime) in space (along and across the strike of the West Africa passive margin) and in time suggest the occurrence of local σ_2 / σ_3 stress permutations possibly related to structural complexities (e. g., Hu and Angelier, 2004).

2.3. The Lower Congo basin: stratigraphy and sedimentology

The Lower Congo basin is located on the eastern margin of the central segment of the South Atlantic between Gabon and Angola (Vernet et al., 1996; Harris, 2000; Aslanian et al., 2009). From the from rifting to the present-day, the basin stratigraphy is divided into three main sections (Fig. 1b): (1) the pre-salt section (145–116 Ma), which is mainly continental, (2) the salt section (118–112 Ma), corresponding to the transitional phase that marks the major incursion of the South Atlantic Ocean into the rift, and (3) the post-salt section (112 Ma to the present day), composed mainly by marine sequences. (McHargue, 1990). The Cretaceous-Cenozoic sedimentary series is directly underlain by the Precambrian “basement” (Fig. 1b & 1c), because the Jurassic, Triassic and Paleozoic series are absent. (Bidiet et al., 1998). The so-called “basement” is composed of both the crystalline part of the Congo craton and the overlying Precambrian pre-rift sediments (Delpomdor et al., 2008; Mbina Mounquengui and Guiraud, 2009; Pr at et al., 2010). Pre-salt basins are mainly filled by fluvial and lacustrine deposits (Guiraud et al., 2010), and have been dated using ostracod biozones, pollens and spores (Grosdidier, 1967; Chaboureau et al., 2013). The pre-salt section is composed of the Neocomian sandstones and clays of the Vandji, Sialivakou, Kouakouala and Djeno formations, and are overlain by the lower Barremian clay of the Pointe Noire (PN) Fm. (Fig. 1b) and the studied TOCA Fm., deposited in a shallow, lacustrine environment (Harris, 2000) during the terminal phase of rifting on top and sides of the Likouala high. Laterally, the TOCA Fm. changes to deeper organic rich shale deposits of Pointe Noire in the Dental and Emeraude basins. The late Barremian clay deposits of the Pointe Indienne Fm. complete the pre-salt section (Harris, 2000).

In this study, we focus on the syn-rift TOCA lacustrine carbonates. On the basis of sedimentological and biological features, Harris (2000) identified three units for the TOCA Fm., from bottom to top: (i) TOCA 1 which is composed of microbialites; (ii) TOCA 2 showing microbial encrustations of shells, microbial mats and thrombolites; and (iii) TOCA 3 made of the accumulation of granular and coquina facies, i.e., mainly freshwater lamellibranch tests belonging to the Unionidae group

(Grosdidier et al., 1996). Recognition of the AS9 ostracod biozone (base AS9 ~ 130 Ma, top AS9 ~ 125 Ma) in the TOCA Fm (Grosdidier et al., 1996; Bate, 1999; Gradstein et al., 2004) suggests a Barremian depositional age.

2.4. The Lower Congo basin: structure

The Lower Congo basin is bounded by two oceanic fracture zones referred to as “arches” (Asmus and Ponte, 1973; Beglinger et al., 2012): the Mayumbe Arch to the north and the Ambriz Arch to the south. The basin rests unconformably on the Mayumbe Precambrian basement to the east (Fig. 1a). The Lower Congo basin includes the onshore coastal basin and the offshore basin which makes most of the margin. In the central Lower Congo basin (Fig. 1a & 2a), the Emeraude and Dentale basins, located on either sides of the Likouala high, represent the depocenters of the syn-rift series (Figs. 1a & 1c).

The map of the top TOCA (top Barremian) (Fig. 2a) shows three main orientations of deep, basement rooted faults at the hectometric to pluri-kilometric scale, consistent with the regional structural pattern in this part of the West Africa margin (Tack et al., 2001). Two of these three orientation groups comprise normal faults oriented N-S and NW-SE (Fig. 2a) (unpublished TotalEnergies report). Both fault strikes can be recognized in the Likouala high and the adjacent basins, but the N-S strike seemingly prevails atop of the high where the TOCA Fm. either never deposited or has been completely eroded, while the NW-SE strike dominates in the areas of the basin where the TOCA Fm. is thicker. The third set, oriented NE–SW, corresponds to transverse faults (Fig. 2a) often referred to as “lineaments” where they are recognized at the larger scale but with poorly-defined vertical offsets on seismics. These transverse lineaments generally line up with onshore features such as paleo-valleys and mapped NE–SW faults and are seen further offshore on gravimetric-magnetic data (unpublished TotalEnergies report). These NE–SW lineaments are considered as a structural expression of margin segmentation during initial northward propagation of the Atlantic rifting.

The data used in this paper come from two offshore wells (Well-1 and Well-2), located ~47 km apart in two distinct domains of the basin on both parts of the Likouala high (Figs. 1 & 2a). The dataset was completed by some fracture orientation data from cores from lateral wells (unpublished TotalEnergies report) (Fig. 2a).

3. Materials and methods

3.1. Studied material

The cores of the TOCA Fm. available for this study are 81 m in length in Well-1 (4069–4150 m) and 9 m in length in Well-2 (2490–2499 m) (Fig. 2b), and they exhibit the same sedimentary facies composed of oncolite limestone locally dolomitized. The studied intervals were selected on their representativity of the sedimentary facies encountered in both well cores.

This study focuses on the TOCA 3 unit which has already been investigated in Well-1 by Bah et al. (2023). In their study, the authors quantified the amount and timing of porosity destruction in the TOCA reservoir. The absolute age of the key paragenetic events controlling reservoir properties have been constrained: mechanical compaction (130–127 Ma based on TemisFlow™ modelling), early cementation (127.4 ± 2.2 to 119.4 ± 6.4 Ma based on U-Pb dating on calcite diagenetic cement), and chemical compaction (117–95 Ma based on sedimentary stylolite roughness inversion). The results reveal that the initial porosity of the TOCA Fm. was reduced down to its current value of 4–8% during the first 35 Ma of its burial history and has not significantly evolved since 95 Ma. Thanks to the early cementation the textures of the TOCA 3 unit display large areas of sparitic calcite grains suitable for calcite twin analysis (Well-1 and Well-2; Fig. 3).

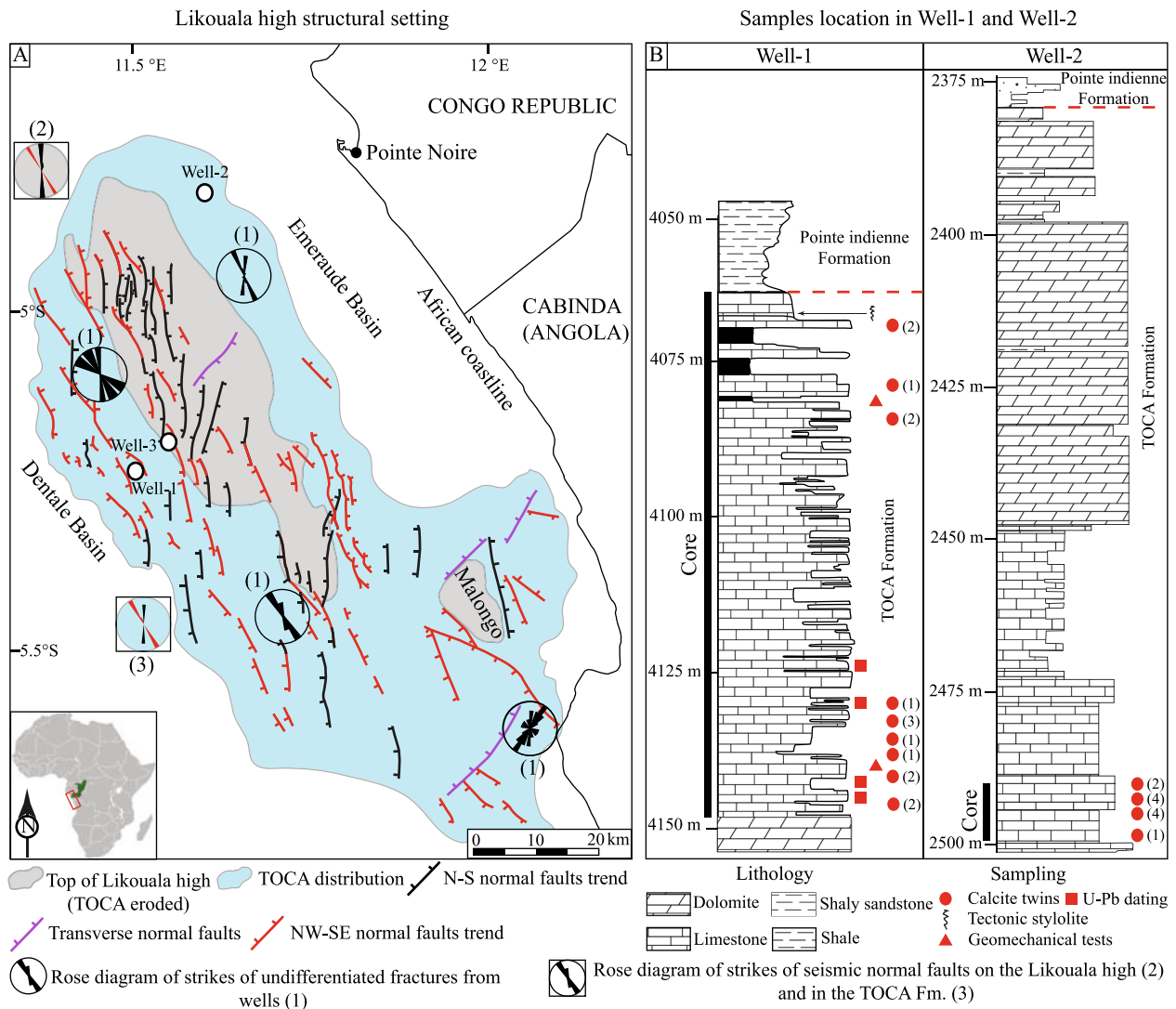


Fig. 2. (A) Main normal faults affecting the TOCA 3 unit and Likouala high basement from unpublished TotalEnergies report. The two rose diagrams in the squares represent the statistical distribution of fault strike (N-S in black and NE-SW in red) on the Likouala high and in the TOCA Fm. Please note that the faults in the Emeraude basin near Well-2 have not been mapped. (B) Schematic stratigraphic chart of the two studied drill cores showing the samples location used in this study. The solid black line shows the cored section for each well. (For interpretation of the references to colour in this figure legend, the reader is referred to the web version of this article.)

3.2. Methods

3.2.1. Optical and cathodoluminescence microscopy

In order to complement the petro-diagenetic description of the TOCA Fm. in Well-1 (Bah et al., 2023), we conducted a petrographic study of the TOCA Fm. in Well-2, based on the analysis of new 36 thin-sections using a Zeiss Axioplot polarizing microscope equipped with a Nikon Digital sight DS_U2/Ds-Fi1 camera. The petrographic phases were observed and identified under unanalyzed polarized light (LPNA) and analyzed polarized light (LPA). The diagenetic state of carbonates was further investigated under cathodoluminescence on a NewTec scientific Cathodyne model CATHOD-SP01 equipped with an IDS UI-3850CP-C-GL R camera (vacuum of 90 mTorr, 12–15 kV voltage and 200 μA intensity). All microscopic work was carried out at the laboratory facilities of the TotalEnergies technical and scientific center (CSTJF, Pau, France).

3.2.2. Strength and failure envelope of the TOCA limestones from mechanical tests

In order to determine the mechanical properties of the TOCA limestones, multiaxial tests were run on two plugs (38 mm in diameter x

76 mm in height) and brazilian tests on two other plugs (38 mm in diameter x 18 mm in height) cut along the vertical axis of the core within the two most frequent textures, namely wackestone and packstone. The principle of the multiaxial test (also referred to as multi-stage test) is the same as the conventional single-stage triaxial test, except that only one test specimen is used for different confining pressures (see Bah et al., 2023 for detail). The results of the tests were used to constrain the elastic properties of the rock (Bah et al., 2023) and to build its intrinsic failure envelope (this study).

3.2.3. Calcite twin inversion for stress applied to oriented cores

Mechanical twinning is a common mechanism of plastic deformation in calcite crystals at low pressure and temperature (Burkhard, 1993; Ferrill et al., 2004; Lacombe et al., 2021a). Twinning occurs by an approximation to simple shear in a specific direction and sense along particular crystallographic *e* planes. Twinning activation is negligibly affected by strain rate, temperature and confining pressure, and depends mainly on differential stress, grain size and strain. (Turner, 1953; Turner et al., 1954; Rowe and Rutter, 1990; Laurent et al., 2000; Lacombe et al., 2021a).

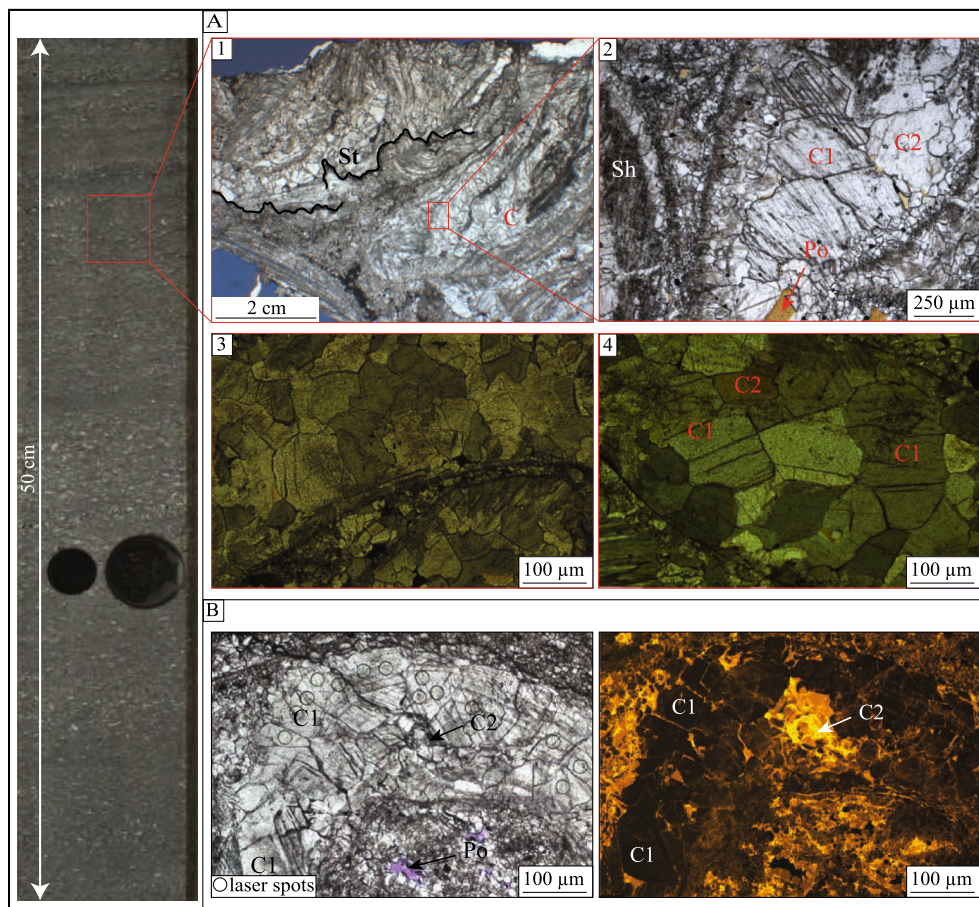


Fig. 3. Photographs of the core showing the studied material. (A) wackestone to packstone texture in Well-1 (A1 & A2) and Well-2 (A3 & A4); (B) Microscopic image in polarized light and cathodoluminescence showing twinned calcite and the different calcite cements. Sh – shells; C1 and C2 – Blocky calcite cement; St – Stylolite.

Calcite twinning paleopiezometry (e.g., Jamison and Spang, 1976; Lacombe and Laurent, 1992; Lacombe, 2007) is a well-established technique to quantify paleostress orientations and magnitudes (e.g., Lacombe et al., 2007, 2009; Craddock et al., 1993; Rocher et al., 1996; Beaudoin et al., 2016; Arboit et al., 2017. See Lacombe, 2010 and Lacombe et al., 2021a for reviews). Inversion of calcite twins for stress is especially appropriate to constrain the paleostress history from limited rock volumes such as cores from wells (e.g., Lacombe et al., 1994; Rocher et al., 2000; Kulikowski and Amrouch, 2017; Zeboudj et al., 2023). In addition to the presence of favorable petro-facies (i.e., sparitic calcite in rock matrix or veins), the technique requires the obvious availability of samples oriented in the geographical frame. For the purpose of paleostress reconstructions, the two investigated cores were oriented either directly in-situ or a posteriori by comparison with the FMS (Formation Micro-Scanner) images of the well.

3.2.3.1. Calcite twin data acquisition. The samples used for calcite twin measurements (Figs. 3 & 4) were spatially oriented as follows: X axis parallel to the generator oriented with respect to north, Y axis parallel to the dip of the core and Z axis perpendicular to the XY plane. Mutually perpendicular thin-sections were cut for each sample from the XY, XZ plane and YZ planes. In each thin section (Fig. 4b), orientations of twin lamellae of optical axes were measured from ~30 crystals using an optical microscope equipped with a Universal Stage with the aid of the software of Tourneret and Laurent (1990). Once acquired, the measurements were restored into the geographical orientation and for each sample, they were plotted to check for the random distribution of the optical axes, hence the absence of any potential bias related to a preferred orientation related to crystal growth or deformation (Fig. 4d).

We also ensured that calcite twins measurements were collected from grains of the same diagenetic phase based on cathodoluminescence images (Fig. 3b).

To estimate roughly twinning strain, we divided the cumulative thickness of all twin lamellae of a given set in a grain by the length of the grain measured perpendicular to the twins. The 2-D grain size in each thin section was determined by adding the length of the long and short axes of the grain and dividing the sum by 2. The resulting grain size histogram allows us to eliminate the outliers, i.e., the under-represented smallest and/or largest size values (Fig. 4d).

3.2.3.2. Calcite twin data inversion for stress. A number of methods of calcite twin inversion for stress have been proposed (e.g., Laurent et al., 1981; Etchecopar, 1984; Laurent et al., 2000; Yamaji, 2015; Parlangeau et al., 2018; see review in Lacombe et al., 2021a). They are based on different principles but share the same conditions of application, i.e., low strain, which warrants coaxiality between stress and strain, and homogeneous stress field at the grain/aggregate scale. Twinning deformation is considered to be irreversible, and twinning occurs if the applied resolved shear stress τ_s is equal to, or greater than, the Critical Resolved Shear Stress for twinning (CRSS) τ_a (Jamison and Spang, 1976; Tullis, 1980; Lacombe and Laurent, 1996; Ferrill, 1998; Laurent et al., 2000; see review and discussion on the meaning of the CRSS in Lacombe et al., 2021a). Thus, one assumes that for twinned planes: $\tau_s \geq \tau_a$ and for untwinned planes: $\tau_s < \tau_a$. Calcite twinning is easier (lower CRSS) in large grains and more difficult (higher CRSS) in small grains. In addition, because calcite hardens once twinned the CRSS increases as twinning strain increases, making further twinning more difficult (Parlangeau et al., 2019; Lacombe et al., 2021a).

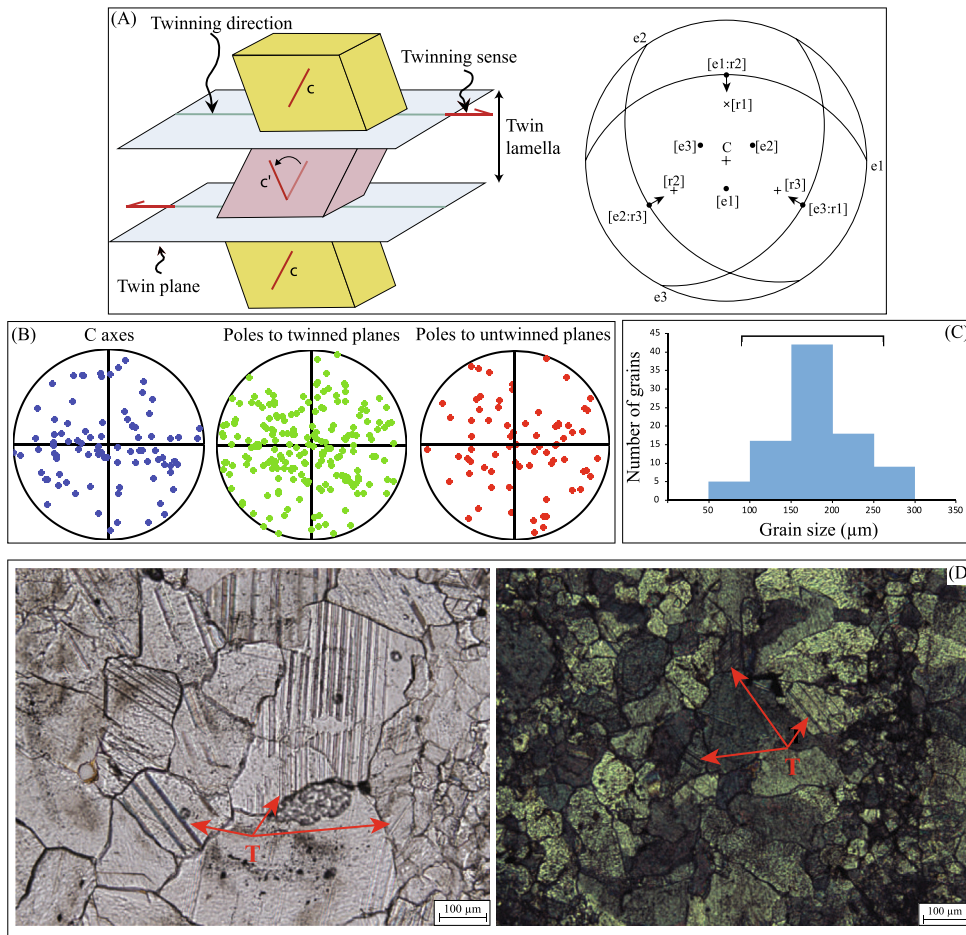


Fig. 4. (A) Schematic and stereographic representation of calcite twinning with the C and C' optical axes of the host crystal and the twinned portion of the crystal (Lacombe et al., 2021a). (B) Example of spatial distribution of optical axes (blue) and poles to twinned (green) and untwinned (red) planes of sample 6 (2493.9 m depth) in Well-2. (C) Example of grain size distribution in the same sample than in B, with the range of grain sizes considered for the CSIT-2. (D) Photographs in natural light of the representative facies in the drill core showing twinned calcite in the matrix in wells 1 & 2 on the left- and right hand side, respectively. T- Twins. (For interpretation of the references to colour in this figure legend, the reader is referred to the web version of this article.)

In this study, we used the stress inversion technique (CSIT-2) developed by Parlangeau et al. (2018) to determine the successive paleostress tensors from the measured twin sets. The principle of the inversion is to determine a stress tensor (or several stress tensors) which verifies the inequalities (1) for the largest number of twinned planes and the whole set of untwinned planes. The solution has the form of a reduced stress tensor with 4 parameters: the orientations of principal stress axes ($\sigma_1, \sigma_2, \sigma_3$) and the stress ratio (Φ):

$$1 \geq \Phi = \frac{\sigma_2 - \sigma_3}{\sigma_1 - \sigma_3} \geq 0 \text{ with } \sigma_1 \geq \sigma_2 \geq \sigma_3 \quad (1)$$

CSIT-2 method allows the presence of one or more tensors to be detected automatically. Considering the complete dataset (twinned and untwinned planes), the first step of the process consists of a systematic search in the 3-D space for the three Euler angles (defining the orientations of the axes of the stress tensors) with a regular interval of 10°, the stress ratio being fixed at 0.5, in order to select the reduced stress tensors accounting for at least 20% of twinned planes. For each tensor, the penalization function f defined as:

$$f = \sum_{j=1}^{j=n} (\tau_s^j - \tau_s^{\min}) \quad (2)$$

with τ_s^j the resolved shear stress applied on the j untwinned planes such as $\tau_s^j \geq \tau_s^{\min}$ and τ_s^{\min} the smallest resolved shear stress applied on the twinned planes compatible with the tensor, is calculated.

From a theoretical point of view, the penalization function is expected to be equal to 0 for a perfect dataset and its value increases with the incorporation of incompatible untwinned planes into the solution. The stress tensors which penalization function is lower than 0.5 are

selected after this first step and each of them is weighted by the number of its nearest neighbours according to a similarity criterion. This enables the rapid and automatic identification of different groups of tensors that are associated with a high percentage of compatible twinned planes and low values of the penalization function. (for more details, see Parlangeau et al., 2018). Each cluster's reference reduced stress tensor is then applied to all twinned and untwinned planes, while the percentages of twinned planes to be explained are gradually increased. The optimal tensor is obtained when 1) the maximum number of twinned planes are taken into account; 2) the minimum number of untwinned planes are taken into account; 3) the value of the penalization function is minimal.

For each stress tensor, the inversion provides the orientation of the principal stress axes ($\sigma_1, \sigma_2, \sigma_3$), the stress ratio (Φ) and a non-dimensional differential stress $\frac{(\sigma_1 - \sigma_3)}{\tau_a}$ which is related to the final value of τ_s^{\min} :

$$\frac{(\sigma_1 - \sigma_3)}{\tau_a} = \frac{1}{\tau_s^{\min}} \quad (3)$$

The choice of the right τ_a value to be used in eq. 3 is of prime importance for the reliable calculation of differential stress magnitudes. In order to estimate the appropriate CRSS value, we rely on the empirical curves proposed by Parlangeau et al. (2019) which reflect the decrease of the CRSS value with increasing grain size (Hall-Petch's rule) and the increase of the CRSS value with strain. Moreover, despite the poor dependence of the CRSS value on temperature, we also paid attention to the range of temperatures of deformation in our samples, considering both the twinning regime (e.g., thin twins denoting twinning at low temperature < 170–200 °C: Ferrill et al., 2004; Lacombe et al., 2021a) and the maximum temperature reached during burial in order to evaluate the possible variations of the CRSS with temperature (De Bresser

and Spiers, 1997; Lacombe et al., 2021a). The τ_a value ultimately retained for calculation is therefore estimated on the basis of the mean grain size and the internal twinning strain of the samples, and to a lesser extent - of the estimated temperature of deformation at each stage of the burial history.

Using the τ_s^{\min} value derived from the inversion process we then determined the values of the differential stresses ($\sigma_1 - \sigma_3$) and ($\sigma_2 - \sigma_3$) using eq. (3), hence the 5 parameters of the deviatoric stress tensor.

The ability of CSIT-2 to detect, separate and determine stress tensors from monophasic and polyphasic twin datasets, including measurements errors or various grain sizes, has been demonstrated by multiple tests on numerically generated twin datasets as well as naturally deformed polyphasic samples (Parlangeau et al., 2018). The associated methodological uncertainty is $\pm 10^\circ$ for the orientations of the principal stresses, ± 0.1 for the stress ratio and $\pm 30\%$ for the values of the differential stresses.

3.3. Burial-time model

In order to reconstruct the burial evolution of the TOCA Fm. over time, we have built a 1-D burial-time model of the TOCA Fm. using TemisFlow™ basin modelling software. In this study we present the burial model for Well-2, which complements the burial model for Well-1 available in Bah et al. (2023). The workflow is summarized below (see Bah et al., 2023 for detail).

The geometry simulation is based on the top-base depths of the formations as measured in Well-2. The properties of each lithology (porosity, permeability) were defined from Well-2 and available seismic interpretations (TotalEnergies internal maps) were used to define the erosional phases to be taken into account, namely the early Aptian erosion (~75 m) related to the peneplanation of the Likouala high during the transition period uplift and the early Tertiary erosion (~100 m) related to the global uplift of the margin. The chronostratigraphic column (Table 1 in Supplementary Material) shows the parameters of the 14 periods modelled for Well-2. Paleo-bathymetry is specified for each period. Additional physical properties such as thermal conductivity, heat capacity and radiogenic production, as well as the compaction constitutive law were defined with respect to the ratio of the different sedimentary textures (limestone, shale, sandstone) described in the layer.

A backstripping process was used to reconstruct the evolution of the basin geometry over time using a 1-D backward modelling. The restoration was performed from the present day to the deposition of the first layer at 145.5 Ma, which corresponds to the age of the basement top. For each period, after removing the overlying layer, the remaining sedimentary formations were decompacted, or compacted (in the case of erosion), by using porosity vs depth curves calibrated empirically for each lithology. The results of the backstripping is the evolution of the thickness with time for each layer.

4. Results

4.1. Petrography of the TOCA limestones

The TOCA Fm. in Well-2 shows the same sedimentary facies and textures than in Well-1 (Bah et al., 2023). Observations on cores and thin-sections reveal two main types of facies: a bioclastic facies (F1) and a mudstone facies (F2). The bioclastic limestone facies is the most common and is composed of broken or preserved unio shells, gastropods and rare oncoids in a microsparitic matrix, occurring as wackestones to floatstones (F1b) and as packstones to rudstones (F1c) (Fig. 3). The less abundant mudstone facies is mainly abiogenic but with sometimes gastropods and ostracods shells. These two microfacies represent about 90% of the cored sections in Well-1 and Well-2, the remaining 10% of the core being composed of grainstones and black shales.

The complete paragenetic sequence of the TOCA Fm. in Well-1 has

been described in Bah et al. (2023). The recognized diagenetic events include, in chronological order, shell micritization, aragonite to calcite neomorphism, precipitation of blocky calcite C1, mechanical compaction, precipitation of blocky calcite C2, and chemical compaction (development of bedding-parallel, sedimentary stylolites). In Well-1, the early blocky calcite cement C1, dated 127.4 ± 2.2 to 119.4 ± 6.4 Ma (Bah et al., 2023), is essentially non-luminescent (dark colour) and developed as an intrabioclast and interstitial cement. The later (unfortunately non dated) calcite cement C2 exhibits a rather bright orange cathodoluminescence and often occurs as overgrowth around C1 crystals or in residual porosity after C1 cementation. The two calcite cements C1 and C2 were also identified in Well-2 on the basis of cathodoluminescence (Fig. 3b); in the two wells, both cements display mechanical twins.

4.2. Strength and failure envelope of the TOCA limestones from mechanical tests

The elastic parameters for the two carbonate textures studied, namely wackestone (F1b) and packstone (F1c), have been reported in Bah et al. (2023). The values of the maximum principal stress σ_1 at 10, 30 and 50 MPa determined from the triaxial tests were used to build the Mohr circles for each loading (Fig. 5). The value of the rock tensile strength was determined from the results of the Brazilian test (Table 2 in Supplementary Material and Fig. 5). The Mohr circles associated with loading and the rock tensile strength enabled us to build the failure envelope for each texture. According to the Mohr-Coulomb criterion, the failure envelope was approximated by a straight line in the positive normal stress domain according to eq. (4):

$$\tau = S_0 + \mu \sigma_n \quad (4)$$

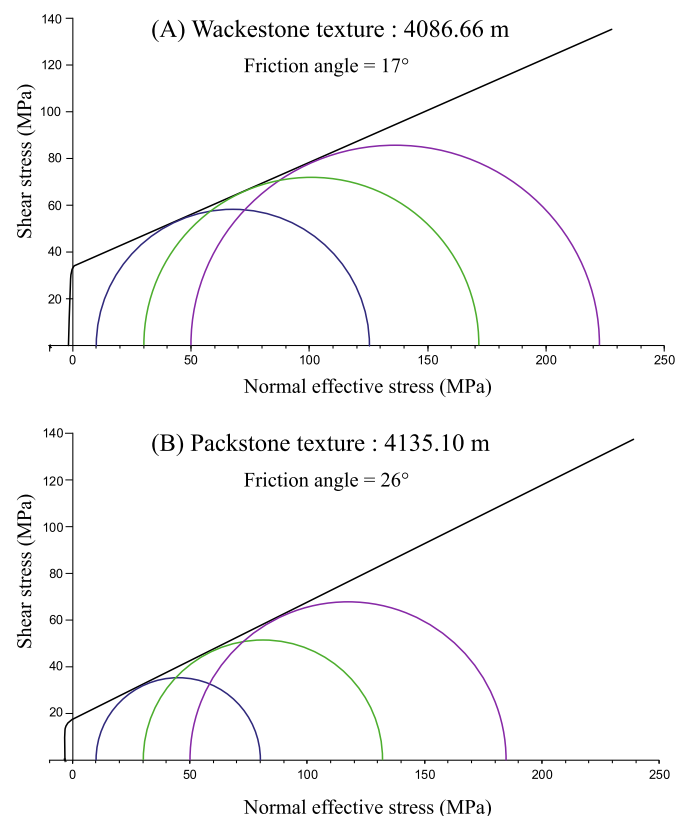


Fig. 5. Mohr diagrams showing the Mohr failure envelope of the TOCA Fm. determined from rock mechanics tests in the wackestone (A) and packstone (B) textures.

with τ the shear stress component, S_0 the cohesion of the material, μ the coefficient of internal friction and σ_n the normal stress component. Brazilian test results which indicate that the rock tensile strength is ~ 1.69 MPa and ~ 3.13 MPa for wackestone (F1b) and packstone (F1c), respectively, were used in the domain of negative normal stress.

It should be noted that the two studied cores did not intersect any visible fractures in the cored section. Although extensional fractures and faults were reported in nearby wells (Fig. 2a), this unfortunate lack of mesoscale brittle structures may be explained by the limited length of cores investigated together with the expected steep dip of the extensional fractures, i.e., oriented nearly parallel to the well axis.

4.3. Results of the inversion of calcite twins for stress

A total of 26 samples were collected in Well-1 and Well-2 in the pre-salt TOCA carbonates at different depths. 15 samples were taken in Well-1 between 4070.25 m and 4148.30 m and 11 samples in Well-2 between 2490.14 m and 2499.25 m. The depth distribution of the samples is shown in Fig. 2 and in the supplementary material. Twins were measured in the C1 cement which displays large blocky calcite crystals. Only a few measurements could be made in the C2 cement due to the small grain size; the resulting twin dataset was unfortunately too limited to carry out a meaningful inversion for stress.

All the twins observed in the samples are very thin ($< 1 \mu\text{m}$) and straight (Fig. 4), and belong to Type I twins (Burkhard, 1993) which indicates that twinning strain remained small (Ferrill et al., 2004; Lacombe et al., 2021a) and occurred at low temperature ($T < \sim 170\text{--}200^\circ$), in agreement with the maximum temperature (Well-1 present-day bottom hole temperature) of 164° reached by the TOCA Fm. during its continuous burial (Bah et al., 2023).

The samples further show a random distribution of optical axes of grains (Fig. 4e), which is a prerequisite for the reliable inversion of calcite twin data for stress. Grain-size histograms for most studied

samples show a distribution of calcite grain sizes between 100 and 350 μm , with a modal value around 200 μm . Only one sample displays smaller grain sizes, with a modal value of around 100 μm . Twinning strain was roughly estimated to be less than 2%. This very small value ensures that twinning strain can be approximated by coaxial conditions so the orientation of twinning strain can be reliably correlated with paleostress orientation (Burkhard, 1993; Amrouch et al., 2010; Wakamori and Yamaji, 2020). The mean grain size and the maximum strain value allowed us to define the appropriate CRSS values to be used for the calculation of the differential stress on the basis of the empirical curves published by Parlangeau et al. (2019) and Lacombe et al. (2021a). These CRSS values were plotted against temperature of deformation to check for consistency. The final CRSS values, between 6 and 7 MPa (except for one sample from Well-2), are reported in Table 3 (Supplementary Material).

Only 6 out of the 26 samples yielded a single stress tensor. All other samples (i.e., $\sim 77\%$) yielded two, three or four superimposed stress tensors. For simplicity, the stress tensors obtained from each well were gathered into different groups on the basis of consistent principal stresses orientations and stress regime (extensional, vertical σ_1 ; compressional, vertical σ_3 ; strike-slip, vertical σ_2) (Fig. 6 and Figs. 1, 2 in Supplementary Material).

Starting from the 56 stress tensors determined from the 26 samples (Table 3, Supplementary Material), a total of 7 main groups of stress tensors could be defined (Fig. 6): three extensional stress tensor groups (A, B and C), two compressional stress tensor groups (D and E), and two strike-slip stress tensor groups (F and G).

For the extensional stress regimes, group A was identified in 10 samples (8 and 2 for Well-1 and Well-2, respectively) and is characterized by a σ_3 oriented $\sim\text{NE-SW}$ and by mean differential stress magnitudes of 50 MPa for $(\sigma_1 - \sigma_3)$ and 20 MPa for $(\sigma_2 - \sigma_3)$. Group B was recognized from 17 samples (12 and 5 for Well-1 and Well-2, respectively), with a σ_3 oriented $\sim\text{N100}$ and mean differential stress

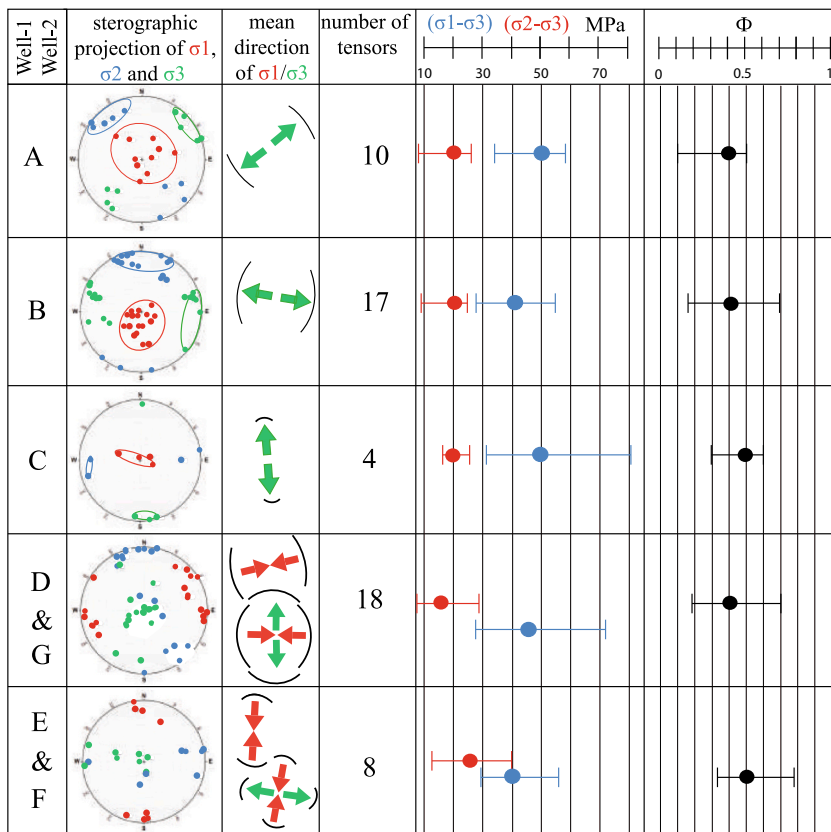


Fig. 6. Summary of stress tensor groups derived from calcite twin inversion using CSIT-2 for Well-1 and Well-2. Each tensor group (from A to G) is characterized by a plot data in stereographic equal-area projection showing the mean orientation of the principal stress axes (red for σ_1 , blue for σ_2 and green for σ_3) and the representation of the average orientation of the horizontal stresses as arrows (red for σ_1 , green for σ_3 , map view). Each tensor group is associated with the number of samples from which the related stress tensors were identified. The average values of the differential stress magnitudes for each group are shown in blue ($\sigma_1 - \sigma_3$) and in red ($\sigma_2 - \sigma_3$) and the average value of stress ratio Φ in black. (For interpretation of the references to colour in this figure legend, the reader is referred to the web version of this article.)

magnitudes of 40 Ma for ($\sigma_1 - \sigma_3$) and 20 MPa for ($\sigma_2 - \sigma_3$). Group C was recognized from 4 samples only (2 and 2 for Well-1 and Well-2, respectively), with a σ_3 oriented ~N-S and mean differential stress magnitudes of 50 Ma for ($\sigma_1 - \sigma_3$) and 20 MPa for ($\sigma_2 - \sigma_3$).

Regarding the compressional stress regimes, group D was recognized from 15 samples (10 and 5 for Well-1 and Well-2, respectively), with a σ_1 oriented ~N70 and mean differential stress magnitudes of 42 Ma for ($\sigma_1 - \sigma_3$) and 15 MPa for ($\sigma_2 - \sigma_3$). Group E was recognized from 6 samples (2 and 4 for Well-1 and Well-2, respectively), with a σ_1 oriented ~N-S and mean differential stress magnitudes of 35 Ma for ($\sigma_1 - \sigma_3$) and 22 MPa for ($\sigma_2 - \sigma_3$).

Regarding the strike-slip stress regimes, groups F and G were identified only in Well-2 from 2 and 3 samples, respectively; they are characterized by a horizontal σ_1 oriented ~N-S (F), and ~ E-W (G) and by mean differential stress magnitudes of 45 MPa for ($\sigma_1 - \sigma_3$) and 28 Ma for ($\sigma_2 - \sigma_3$) for F, and 48 MPa for ($\sigma_1 - \sigma_3$) and 22 MPa for ($\sigma_2 - \sigma_3$) for G.

4.4. Burial-time model

The burial-time model developed for Well-2 (Fig. 9) is very similar to that published for Well-1 (Bah et al., 2023). It shows five phases of burial evolution over time: (1) 130 Ma to 118 Ma, a first phase of moderate

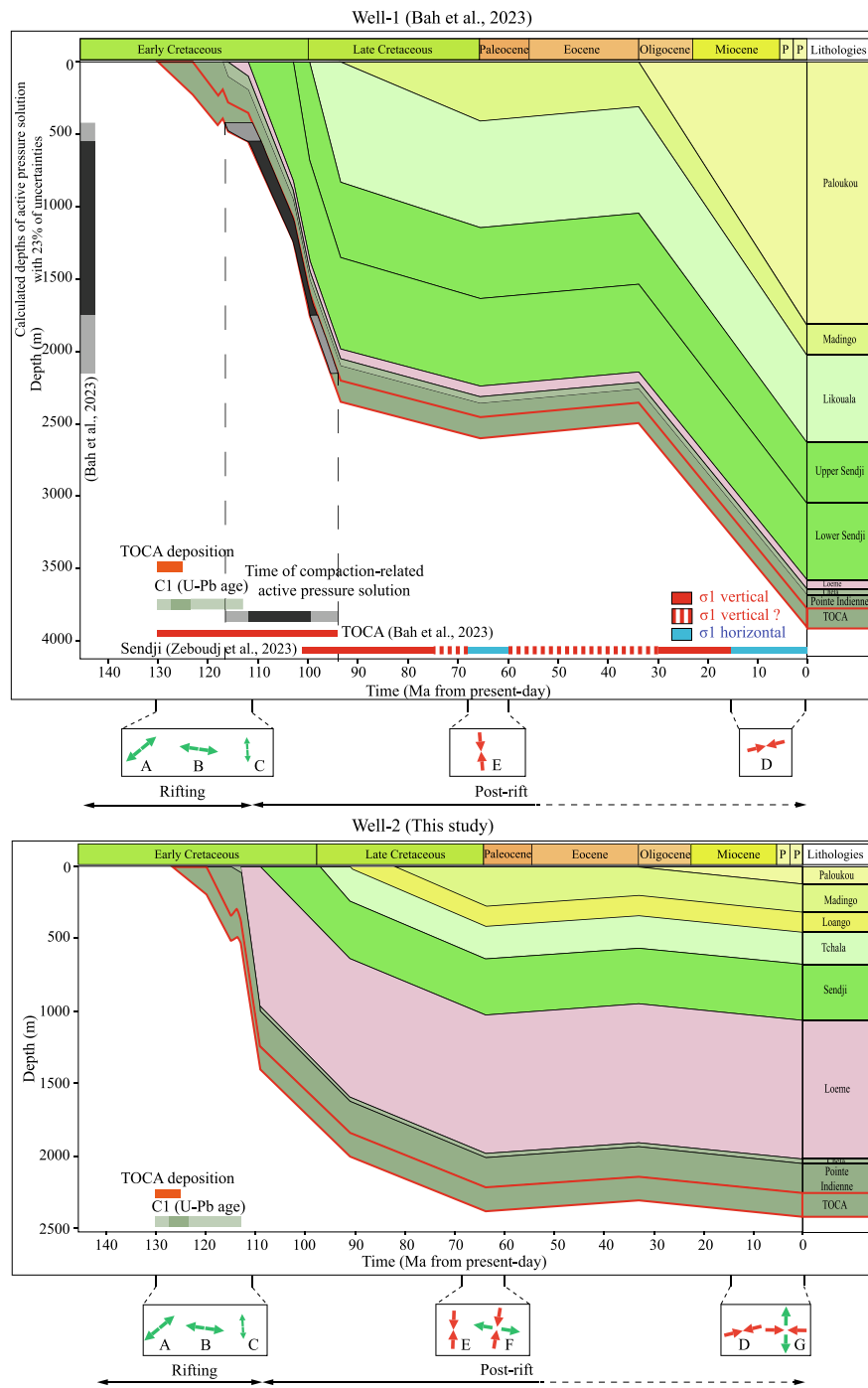


Fig. 7. Burial model constructed from Well-1 (Bah et al., 2023) and Well-2 data corrected for mechanical compaction. The depth on the model is counted from the sea-bed. The calculated depth range of active pressure-solution from bedding-parallel stylolite inversion is reported for the TOCA Fm. as black/grey levels on the y-axis. The stress regimes revealed inversion of calcite twins were also reported (map view).

burial (~25 m/Ma) during the early Cretaceous rifting episode followed by a 75 m erosion. This erosional event observed at 118–117 Ma represents a margin uplift with a peneplanation event (see Fig. 1b). The second phase corresponds to a rapid deposition of sandstones and evaporites with an average burial rate of 197 m/Ma during the transition phase. The post-rift phase starts with (3) a moderate burial rate (~22 m/Ma) from 112 Ma to 63 Ma, followed by (4) a moderate uplift (63 Ma to 35 Ma), leading to a moderate erosion in the lower Tertiary, and ends by (5) a third phase of gentle burial (~3.5 m/Ma) from 35 Ma to present day.

The comparison between the Well-2 and Well-1 models (Fig. 7) shows that the burial rates of the first phase during the early Cretaceous rifting are in the same order of magnitude. Although the thickness of the Loeme salt is very different in the two wells due to the pre-salt paleotopography and to the salt migration during salt tectonics, the strong post-rift subsidence is also of the same order of magnitude, while slightly delayed in time for Well-1 on the Likouala high. The Late Cretaceous quiescence is the same but the Oligo-Miocene burial is much higher on the slope of the margin (Well-1).

5. Discussion

Hereinafter, the reconstructed successive paleostress orientations are discussed in the Africa-fixed reference through time.

5.1. Timing of the reconstructed paleostress regimes

The results of the inversion of calcite twins document a complex, polyphase paleostress history. The depositional age of the TOCA Fm. derived from biostratigraphy (Grosdidier et al., 1996) and the absolute U-Pb dating of the C1 calcite cement (127.4 ± 2.2 to 119.4 ± 6.4 Ma, Bah et al., 2023) from which twin measurements were taken provide time constraints on the beginning of the evolution (Fig. 7).

The distribution of depth ranges of sedimentary stylolite activity projected onto the burial-time curves provides the time periods of compaction-related active pressure-solution, hence the periods dominated by a stress regime with a vertical σ_1 (Bah et al., 2023) (Fig. 7). Because sedimentary stylolites develop under a vertical σ_1 , the maximum depth of active pressure solution can be interpreted as the depth (and so the time once projected onto the burial model) at which σ_1 switched from vertical to horizontal as a result of the horizontal tectonic stress becoming large enough to overcome the vertical stress. This idea has been illustrated and validated in foreland fold-and-thrust belts (Beaudoin et al., 2020; Labeur et al., 2021; Lacombe et al., 2021b). At passive margins, it is sound to consider that the halt in sedimentary stylolite development can alternatively be due to reservoir scale fluid overpressure, possibly related to hydrocarbon migration (Schoellkopf and Patterson, 2000; Brownfield and Charpentier, 2006; Beglinger et al., 2012; Bah et al., 2023). Whatever the reason of the end of stylolite development, this places significant constraints on the time periods when the σ_1 was vertical, i.e., until 95 Ma at least (Fig. 7). As a result, the time periods for which there is no positive evidence of vertical σ_1 as ascertained by active stylolitization are potentially those periods when horizontal σ_1 was prevailing, which constrain the possible timing of strike-slip and compressional stress regimes recorded by calcite twinning. For the part of the story which is not directly constrained by our dataset, we used the results from Zeboudj et al. (2023) on the post-rift carbonates of the Sendji Fm. (Well-3 on Fig. 1), which recorded a longer history of compaction-related pressure solution than the TOCA Fm. These results, combined with basin-scale fault patterns and with earlier onshore paleostress reconstructions along the passive margins of West and South Africa, enabled us to propose a consistent regional (paleo)stress and tectonic evolution over time since the deposition of the syn-rift TOCA Fm.

5.1.1. Timing and sequence of extensional paleostresses and normal faulting

On the basis of the results of the inversion of the roughness of the sedimentary stylolites in the TOCA Fm. of Well-1 (Bah et al., 2023) and the known age of the onset of rifting (Beglinger et al., 2012; Salomon et al., 2015), one can state that the stress regime has been dominated by a vertical σ_1 from ~130 Ma (age of basal TOCA Fm.) until at least 95 Ma. From 95 Ma to the present day, there is no direct evidence of compaction-related pressure solution in the TOCA Fm. We, therefore, propose that the extensional paleostresses recorded by calcite twinning (stress tensor groups A, B and C) be dated between ~130 (earlier absolute age of C1 cement considering uncertainties) and 95 Ma, and more probably between 130 and ~112 Ma (end of rifting). From ~112 Ma to 95 Ma, burial stress and related vertical compaction likely dominated, with no evidence of horizontal extension.

In order to establish the sequence of the extensional stress regimes, we compared the reconstructed extensional trends with the pattern of basin-scale normal faults in the Lower Congo basin. The map of the top TOCA (Fig. 2a) shows that the N-S normal faults are observed mainly atop of the Likouala high where the TOCA Fm. was non deposited or totally eroded, but also affect the TOCA Fm. where present. The NW-SE normal faults are found mainly where the TOCA Fm. is present and to a minor extent on the eroded top of the Likouala high; they represent the dominant set of faults bounding the NW-SE oriented Likouala high. At the mesoscale, the fracture sets described in the TOCA section of other wells in the vicinity of the Likouala high and reaching the base of the TOCA Fm. (rose diagrams Fig. 2a, unpublished TotalEnergies reports) show a strike distribution of high angle (extensional) faults from N-S to NW-SE with a dominance of the NW-SE strike, in agreement with the regional fault patterns (Mbinda Mounguengui and Guiraud, 2009).

The above pattern of normal faults suggests that the N-S normal faults were active before and during the deposition of the TOCA Fm. while the NW-SE normal faults have been mainly active during deposition of the TOCA Fm. This would imply that both normal fault sets were active during the TOCA Fm. deposition, but that the activity of the N-S faults predated that of the NW-SE faults. The consistency of the stress tensor group A (NE-SW extension) with the kinematics of the dominant NW-SE striking normal faults on the one hand, and of the stress tensor group B (N100 to WNW-ESE extension) with the kinematics of the ~N-S fault sets on the other hand, confirms that both groups of tensors reflect extensional events associated with continental rifting between 130 and 112 Ma. We propose that the N100 extension dominated in the Lower Congo Basin during the early continental rupture in relation to the development of the N-S striking normal faults, and that the extension direction subsequently evolved during the Barremian into the regional NE-SW trend associated with the development of the NW-SE striking normal faults leading to the opening of the South Atlantic. The timing of the N-S trend (stress tensor group C) remains unconstrained.

5.1.2. Timing and sequence of strike-slip and compressional paleostresses

The absence of any constraint on the attitude of σ_1 after 95 Ma leaves room for the interpretation on the timing of the stress tensor groups D, E, F and G associated with horizontal σ_1 as obtained by inversion of calcite twins and that we interpret as post-rift paleostresses. After 95 Ma, either σ_1 has switched to horizontal, meaning that tectonic stresses overcame the vertical stress related to burial so vertical compaction ended, or for some reason (e.g., massive cementation/clogging of porosity, fluid overpressure) chemical compaction in the TOCA Fm. ceased (Bah et al., 2023) while σ_1 was still vertical.

Our results therefore suggest a post-95 Ma age for the stress regimes with horizontal σ_1 oriented either ~N-S (stress tensor groups E and F) or ENE-WSW to E-W (stress tensor groups D and G). Noticeably, during the period of time starting at ~95 Ma and running until 33 Ma, the burial rate strongly slowed down and the reservoir even uplifted (between 66 and 33 Ma, Fig. 7). Because the N-S compression has a trend and a possible timing consistent with the latest Cretaceous-Paleocene

compression described by Guiraud and Bosworth (1997), we tentatively propose to assign a latest Cretaceous-early Paleocene age (~67–60 Ma) to the stress tensor groups (E and F). This late Cretaceous-Paleocene compression therefore would be concomitant with the onset of the Paleogene margin uplift (Fig. 7), even though a causal link between these two events remains difficult to ascertain.

The compressional and strike-slip stress tensor groups (D and G, respectively) are both associated with horizontal σ_1 oriented ENE-WSW and E-W, respectively, hence are consistent with the present-day stress (Figs. 1 and 8; Heidebach et al., 2016; Nkodia et al., 2022). We, therefore, propose to relate these stress tensor groups, as well as the development of the sole tectonic stylolite documented in the core which exhibits horizontal peaks oriented ~N100 (Fig. 2), to the same state of stress than the present-day one. However, our results alone do not enable us to precisely date since when these strike-slip and/or compressional states of stress prevailed.

Calcite twin analyses from the TOCA Fm. (this study) and from the supra-salt Sendji Fm. (Zeboudj et al., 2023) yield similar results on most of the post-rift paleostress record (Figs. 7 and 8). The major difference between the stress records in the two formations is (1) that the syn-rift TOCA Fm. recorded the extensional stresses related to rifting, and (2) that the supra-salt Sendji Fm. recorded the post-rift halokinesis and related paleostresses that were not recorded in the pre-salt TOCA Fm. While being aware of these differences, one can combine the results of the two studies to better constrain the timing of the compressional and strike-slip stress tensor groups. The inversion of the roughness of sedimentary stylolites in the post-salt Sendji Fm. (Zeboudj et al., 2023) indicates that most compaction-related stylolitization has been active between 102 and 15 Ma. After ~15 Ma, no sedimentary stylolite seems to have developed, which suggests that a stress regime with σ_1 horizontal (either strike-slip or compressional in type) prevailed since then. We therefore assign a post ~15 Ma (post 15–10 Ma to be conservative taking into account uncertainties, Zeboudj et al., 2023) to the stress tensor groups D and G. Because the present-day stress regime is rather compressional (Figs. 1A and 11), we propose that the period dominated by a σ_1 horizontal oriented ENE-WSW to E-W started under a strike-slip stress regime (stress tensor group G) and evolved through time into a compressional stress regime (stress tensor group D), keeping in mind the probable occurrence of σ_2 / σ_3 stress permutations in space (along and across the strike of the margin) and time (since 15 Ma).

5.2. Regional significance of the reconstructed paleostress regimes

5.2.1. Extensional paleostress regimes and the syn-rift tectonic history of the West Africa passive margin

The comparison between the extensional trends derived from inversion of calcite twins and the pattern of normal faults suggest that in the Lower Congo basin, the early syn-rift extension was oriented N100 in relation to the development of N-S striking normal faults, then evolved into the regional NE-SW extension associated with the development of the dominant pattern of NW-SE striking normal faults. A possible explanation for the change in normal fault strike and associated extensional trends during rifting consists in the influence of structural inheritance, especially the geometry of the Neoproterozoic basement structures, on the development of later extensional structures. The Mayumbe belt underlying the Lower Congo basin is dominated by NNW-SSE trending foliation (Pedrosa-Soares et al., 1992; Affaton et al., 2016), while the Kaoko belt in Namibia is dominated by approximately N-S trending foliation (e.g., Passchier et al., 2002; Goscombe and Gray, 2008). These inherited basement weaknesses were favorably oriented for extensional reactivation under an N100 to NE-SW extension. We therefore propose that the syn-rift extension first had a N100 trend and was associated with the early development of N-S striking normal faults owing to the reactivation of preexisting basement weaknesses, then evolved during the Barremian into the dominant NE-SW extension leading to opening of the South Atlantic. The N-S extension (stress tensor

group C) was identified only in very few samples (Figs. 7 and 8), which would suggest a limited regional importance; we propose that this N-S extension, which is consistent with the few E-W (to ENE-WSW) striking normal faults that possibly acted as transfer faults during rifting (Fig. 2a), may reflect a local state of stress at the basin scale.

Alternatively, one could propose that whereas the NE-SW extension (Fig. 8) reflects the divergent motion between the African and South American plates (i.e., the boundary conditions), additional lithospheric doming related to mantle upwelling during rifting may have caused second-order radial pattern of gravitational extensional trends. Salomon et al. (2015) reported two extensional directions for the South Atlantic rifting episode derived from the analysis of mesoscale striated faults in Namibia (Fig. 8), and proposed that the diversity of extensional directions during rifting may have resulted from the combined effects of flexural bending due to sediment loading offshore and continuous upwelling of the African superplume that remained located below the African continent after the break-up of Gondwana (Braun et al., 2014). Although this scenario of a plume-related lithospheric doming should not be overlooked, we favor the role of crustal structural inheritance and of possibly changing boundary conditions (e.g., divergence between Africa and South America) as the more likely explanation of the changing extensional trends in the Lower Congo basin during rifting.

5.2.2. Compressional and strike-slip paleostress regimes and the (complex) post-rift tectonic history of the West Africa passive margin

During the post-rift evolution of the South Atlantic Ocean, several states of stress, either strike-slip or compressional in type, have been recorded along the central and southern West Africa margin (Fig. 8). This result is in line with the findings by Withjack et al. (1995) that passive margins may not have a simple two-stage evolution of rifting and drifting, but instead may have experienced a complex tectonic history including extension and shortening during passive margin development.

Our interpretation that the post-95 Ma ~ N-S compressional trend corresponds to the latest Cretaceous-Paleocene (~67–60 Ma) compression described by Guiraud and Bosworth (1997) suggests that compressional stresses generated at the distant Africa-Eurasia plate boundary were transferred far across the African plate (Figs. 7 and 8). This far-field stress transmission would likely require a deep stress guide, such as a high strength (rigid) continental lithosphere. This hypothesis is in line with the observation of similar compressional trends in the pre-salt section of Well-1 and Well-2 located on both sides of the Likouala high, as well as in the post-rift, supra-salt Sendji Fm. of Well-3 after welding of the supra-salt formations due to salt removal (Zeboudj et al., 2023).

The reconstructed strike-slip and compressional stress regimes with horizontal σ_1 trending ENE-WSW to E-W are consistent with the present-day stress regime (Fig. 8) (Delvaux and Barth, 2010; Heidebach et al., 2016; Nkodia et al., 2022). Zeboudj et al. (2023) have tentatively associated this stress regime with an intraplate ~E-W compression prevailing from the Miocene (~15 Ma) onwards and possibly related to the Atlantic ridge push effect (Fig. 8). We also propose that the compressional / strike-slip stress regimes with σ_1 oriented ENE-WSW to E-W be related to a far-field effect of the mid-Atlantic ridge push, prevailing from ~15 Ma onwards. This interpretation is consistent with the idea that the ridge push could have efficiently controlled the lithospheric stress long after the initiation of the spreading ridge (e.g., Wiens and Stein, 1983, 1985). If this interpretation is correct, our results would support a transmission of the ridge push-related compressional stress over a large distance (~2500 km between the oceanic ridge and the study area since ~15 Ma). This interpretation is in line with the numerical models of Mahatsente and Coblenz (2015) that show that the magnitude of the Atlantic ridge-push force is significantly less than the integrated strength of the oceanic part of the African (Nubian) plate, so this part of the plate is very little deformed and the stresses related to the ridge push can be transferred far into the interior of the oceanic and continental parts of the African plate. Our results also agree with the

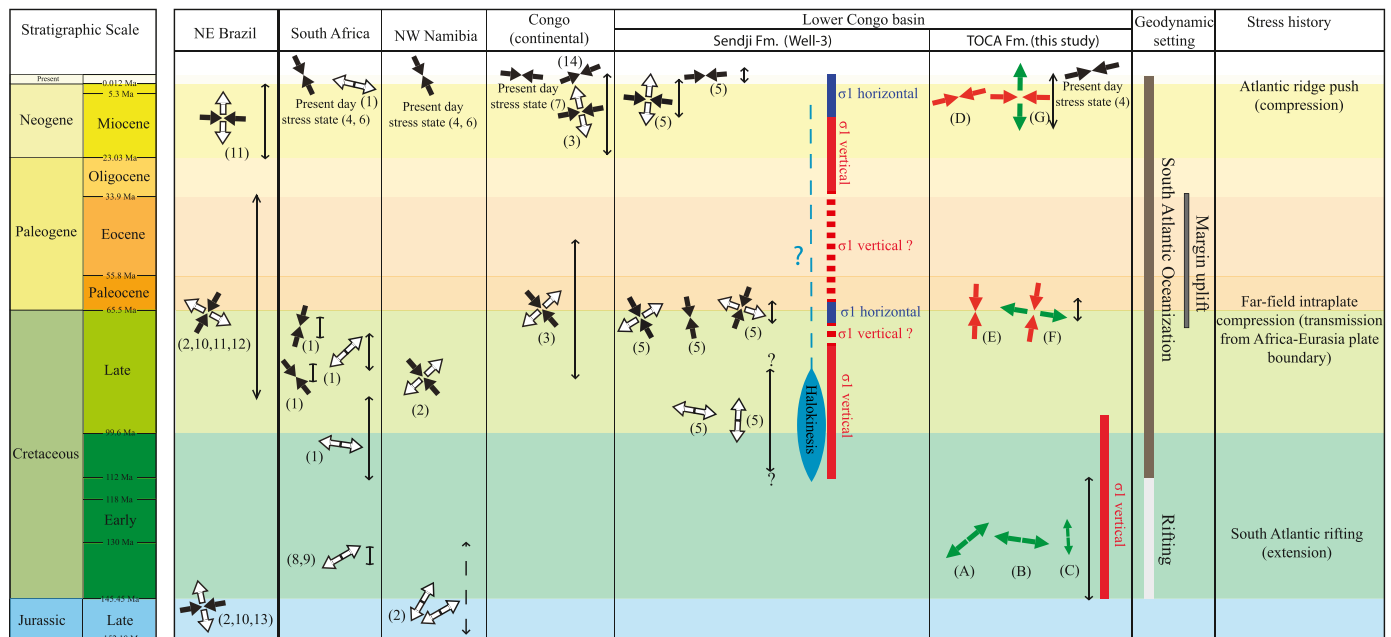


Fig. 8. Summary of the time distribution of tectonic events and associated stress orientations (projected onto the present position of Africa in map view) since early Cretaceous to present recorded in the southern West Africa (Congo, Namibia, Angola and South Africa) and Brazil. (1) Viola et al., 2012; (2) Salomon et al., 2015; (3) Nkodia et al., 2020; (4) Heidbach et al., 2016; (5) Zeboudj et al., 2023; (6) Viola et al., 2005; (7) Delvaux and Barth, 2010; (8) Rabinowitz and LaBrecque, 1979; (9) Nurnberg and Müller, 1991; (10) Riccomini, 1995; (11) Fernandes and Amaral, 2002; (12) Machado et al., 2012; (13) Ferrari, 2001; (14) Nkodia et al., 2022.

findings of Withjack et al. (1995) that during the development of the southeastern Canadian passive margin, the Fundy rift basin on the western edge of the margin experienced shortening possibly associated with sea-floor spreading processes such as ridge push or continental resistance to plate motion. Recently, Nkodia et al. (2022) proposed that the present-day stress pattern in the Lower Congo basin (offshore Angola) could be related to stress loading of the passive margin and interior Congo by the oceanic transform faults extending onland, which would trigger the reactivation of well oriented faults systems. In this scenario, the present-day stress pattern would not be strictly controlled by the ridge push but would still be related to a sea-floor spreading process. However, alternate stress sources also may have contributed to the late Tertiary-present stress field in the West Africa passive margin. Some modelling studies (e.g., Medvedev, 2016) suggest that in addition to the ridge push effect other stress sources (e.g., density variations within the lithosphere, flexural loading of the lithosphere) are involved throughout the African plate. This mixed origin of the recent/contemporary stress pattern would be in agreement with the results of Pascal and Cloetingh (2009).

Our stress results do not allow the formal recognition of the post-rift Campanian-Maastrichtian NE-SW extension that Guiraud and Bosworth (1997) consider as an Africa-wide extensional event. Possible explanations include (1) the weak transmission of far-field extensional stresses into the investigated offshore part of the margin, or (2) the inability of our calcite-twin dataset to discriminate among the superimposed effects of this extensional stress and of the rifting-related extensional stresses. The reason why the late Santonian (~83–85 Ma) N-S to NW-SE compression described by Guiraud and Bosworth (1997) has not been recorded by calcite twinning in our samples from the Lower Congo basin (Zeboudj et al., 2023; this study) while it was seemingly identified in Namibia and South Africa (Viola et al., 2012; Salomon et al., 2015) remains unclear at this time.

To sum up, during its post-rift tectonic history, the West Africa passive margin underwent compressional and/or strike-slip stress regimes, being either tectonic (compressional stress transfer from the distant collisional Africa-Eurasia plate boundary) or gravitational (ridge push transmitted from the mid-Atlantic ridge) origins. Our

interpretations are consistent with earlier claims that the late Cretaceous–Cenozoic intraplate contractional deformation at the Norwegian continental shelf was possibly related to far-field effects of active plate-margin processes and transfer of stresses across the plate as a consequence of the sub Hercynian and Paleocene ‘Laramide’ event of the Alpine orogeny, with additional significant contribution of ridge push from the North Atlantic spreading particularly during the Neogene (Vagnes et al., 1998).

5.2.3. (Paleo)stress evolution of the Lower Congo Basin and tectonic history of the West Africa passive margin in the framework of the Barremian to present-day kinematic history of Africa and South Atlantic

Several kinematic reconstructions have been proposed for the opening of the South Atlantic based on paleomagnetic data (Bullard, 1965; Vink, 1982; Torsvik et al., 2009a, 2009b; Aslanian et al., 2009; Heine et al., 2013; Pérez-Díaz and Eagles, 2014). All reconstructions involve a relative motion of South America with respect to fixed Africa combining both a clockwise rotation of ~40–45° and a translation. The different reconstructions are quite similar since the onset of oceanic spreading (112 Ma), but may show significant differences for the rifting phase (see discussions in Aslanian and Moulin, 2010; Moulin et al., 2010; Chaboureaud et al., 2013; Pérez-Díaz and Eagles, 2014), mainly due to the difficulty of having reliable markers to constrain the exact position of Africa and South America at the onset of rifting.

The main stages of the paleostress and tectonic evolution of the central segment of the West Africa passive margin as recorded by the TOCA Fm. are reported on a series of paleogeographic maps (considering Africa fixed) spanning from the Barremian to the present (Fig. 9). These maps are based on the kinematic reconstructions of Heine et al. (2013) for the rifting episode and the onset of oceanization (Barremian to Albian) and of Moulin et al. (2010) for the Paleocene until the present because the reconstructions of Heine et al. are not available after 100 Ma.

In the early Barremian (130 Ma, Fig. 9a), the extension between Africa and South America that was initiated in the Neocomian continued while the carbonates of the TOCA Fm. started to be deposited in a continental lacustrine environment. In the late Barremian (127 Ma,

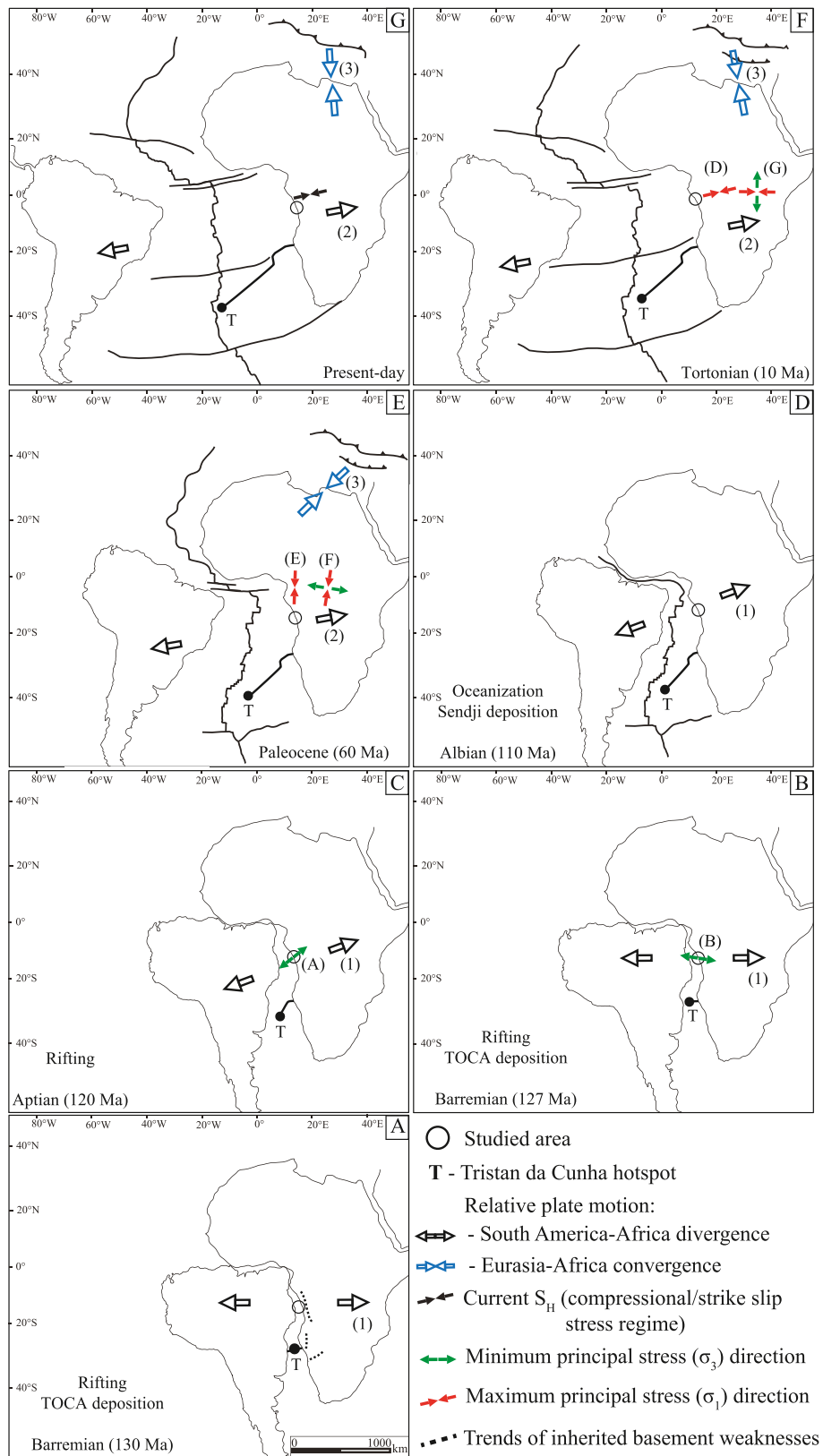


Fig. 9. Paleogeographic reconstruction maps on which the directions of the paleostresses resulting from the inversion of the calcite twins are plotted in map view (see text for more details). (1) Heine et al., 2013; (2) Muller et al., 2016; (3) Jolivet et al., 2021.

Fig. 9b), an ~N100 extension prevailed in the Lower Congo basin, associated with the reactivation of pre-existing basement structures and the formation of N-S striking normal faults (Fig. 9). The likely minor ~N-S extension which could be related either to reactivation of the transverse faults within the basin or to a σ_2 / σ_3 stress permutation during N100 extension has not been plotted. The reconstructions by Heine et al. (2013) involve an E-W divergent motion between Africa and South America at 132 Ma changing to a NE-SW divergent motion at 126 Ma. Considering the deposition age of the TOCA Fm. and the age of the C1 cement from which calcite twin measurements were taken, a (progressive?) change from N100 to NE-SW extension occurring at ~126 Ma would be consistent with both our paleostress results and the observed normal fault pattern in the Lower Congo basin.

In the Aptian (120 Ma, Fig. 9c), continental rifting continued and propagated northwards. A NE-SW extension prevails in the Lower Congo Basin (Fig. 9), associated with the activity of the major NW-SE normal faults. This NE-SW extension likely controlled the structural geometry of the central segment of the West Africa passive margin.

In the Albian (110 Ma, Fig. 9d), sea-floor spreading started to be active and the Sendji Fm. deposited while the extension continued in the Equatorial Atlantic (Loparev et al., 2021).

In the early Paleocene (60 Ma, Fig. 9e), while the spreading of the South Atlantic was active, the stress regime of the West African passive margin became transiently compressional or strike-slip in type with σ_1 oriented ~N-S. This state of stress possibly reflects a far-field compressional stress transfer from the distant active Africa-Eurasia convergent plate boundary.

From the middle Miocene (Fig. 9f) to present (Fig. 9g), the prevailing stress regime along the west Africa passive margin is mainly compressional or strike-slip with σ_1 oriented ENE-WSW to E-W and is thought to originate mainly from the mid-Atlantic ridge push (Fig. 9).

5.3. Paleostress magnitude and implications for fracture prediction in the TOCA Fm

The consideration on the attitude of σ_1 derived from sedimentary stylolite roughness paleopiezometry combined with burial-time evolution of the TOCA Fm. (Bah et al., 2023) and the Sendji Fm (Zeboudj et al., 2023) helps unlock the full determination of principal stress magnitudes which requires the knowledge of the burial depth of the rocks at the time of deformation (Beaudoin and Lacombe, 2018). Hereinafter, the differential stress values provided by calcite twin paleopiezometry are combined with the vertical stress estimates derived from the burial model to estimate principal stress magnitude at the time of deformation (Lacombe and Laurent, 1992; Lacombe, 2007). The resulting principal stress magnitudes are further compared with the strength of the intact whole rock derived from geomechanical tests (i.e., failure envelope) to evaluate the consistency of the stress results and to help predict whether fracturing can be expected in the reservoir under the reconstructed paleostresses. We also compare the paleostress magnitudes related to *syn*-rift extension and post-rift compressions recorded by the TOCA Fm. in the two wells (Well-1 and Well-2) in which the final burial depths of the TOCA Fm. are different, as well as the paleostress magnitudes related to post-rift compressions in the TOCA Fm. in Well-1 and in the Sendji Fm. in Well-3 (Zeboudj et al., 2023) (Fig. 10) because the two formations reached nearly similar final burial depths. For this purpose, the value of σ_v was calculated at the time the paleostress of interest prevailed, assuming either dry conditions $\sigma_v = \rho gh$ or hydrostatic fluid pressure $\sigma_v = (\rho - \rho_w)gh$, with ρ the dry density of the rock column above (2600 kg.m^{-3}), ρ_w the density of water (1000 kg.m^{-3}), g the gravitational field acceleration (9.81 m.s^{-2}), and h the depth (m). Hereafter, we consider that the tangency of the (σ_1 - σ_3) Mohr circle to the failure envelope is indicative of rock failure.

The lower Cretaceous extensional tectonic events was recorded by calcite twins (stress tensor groups A, B and C) when the TOCA Fm. was buried at maximum ~500 m and ~ 1000 m depth in Well-1 and Well-2,

respectively (Fig. 7). These burial depths correspond to mean values of 14 MPa and 28 MPa for the vertical stress σ_1 in dry conditions for Well-1 and Well-2, respectively. The values of the principal stresses σ_2 and σ_3 are then deduced from the differential stress values (σ_1 - σ_3) and (σ_2 - σ_3) (Fig. 6 and Figs. 1, 2 in Supplementary Material). For dry conditions, the value of σ_3 is negative (i.e., in the tensile domain on the Mohr diagram; Fig. 10) for both stress regimes and in both wells, and its absolute value is even larger than the rock tensile strength as indicated by geomechanical tests, so the corresponding Mohr circle exceeds the strength envelope of the intact rock. The assumption of a hydrostatic fluid pressure would lead to even more negative effective stress values of σ_3 , which is impossible. This means that the differential stresses related to the extensional stress regimes are possibly overestimated, even when considering the possible uncertainties on their values ($\pm 30\%$, Fig. 10). In contrast, differential stress magnitudes for compressional and strike-slip stress regimes are in line with expected shallow crustal stresses (Lacombe, 2001, 2007; Beaudoin and Lacombe, 2018). Lacombe et al. (1990), Lacombe et al., 1994) already reported abnormally high differential stress magnitudes related to Eocene-Oligocene extension in the Paris basin, that Lacombe and Laurent (1992) tentatively related to the superimposition of extensional paleostress tensors that the method could hardly discriminate. One possible explanation would be that the calcite twin population which recorded the extensional stress regimes actually formed not only during rifting, but also during continuing post-rift burial as long as the vertical principal stress σ_1 was vertical. In other words, a longer duration of the application of a causative differential stress would have allowed for the cumulative development of twins within randomly oriented grains less favorably oriented to twin (Lacombe et al., 2021a). This means that the unexpectedly high differential stress values returned by calcite twin analysis for extensional stress groups might possibly result from the superimposed effects of differential stress related to *syn*-rift extension and of the differential stress related to later post-rift burial under a vertical principal stress σ_1 that prevailed at least until 95 Ma (Bah et al., 2023).

To test this hypothesis and to estimate the theoretical possible contribution of post-rift burial on the differential stress values for the extensional stress regimes, we assumed that the effect of burial can be approximated by a state of stress with $\sigma_1 > \sigma_h = \sigma_H (= \sigma_2 = \sigma_3)$. This is more likely the case during the burial of the TOCA Fm. between 112 and 95 Ma, i.e., after the rifting. In contrast, during the rifting period, this assumption is theoretically incorrect since calcite twinning paleopiezometry indicates that (σ_2 - σ_3) values are about 15–20 MPa (Fig. 6 and Figs. 1, 2 in Supplementary Material).

The burial-time model (Fig. 7) performed on Well-1 and Well-2 indicates that the TOCA Fm. was buried from ~500 m depth at 112 Ma (end of rifting) to ~2100 m at 95 Ma in Well-1 and from ~1000 m depth at 112 Ma to ~1860 m at 95 Ma in Well-2. The depth difference, ~1600 m and ~ 860 m in Well-1 and Well-2, respectively, was used to calculate the corresponding range of values for $\sigma_v = \sigma_1$. The resulting vertical stress is ~41 MPa and ~ 22 Ma for Well-1 and Well-2, respectively. Considering these values and the mean Poisson ratio of the TOCA limestones determined from geomechanical tests (see section 4.2), and assuming uniaxial strain, we use eq. (5):

$$\sigma_H = \sigma_h = \left(\frac{\nu}{1-\nu} \right) \sigma_v \quad (5)$$

to derive a burial-related maximum differential stress magnitude (σ_v - σ_h) of ~30 MPa and ~ 15 MPa for Well-1 and Well-2, respectively between 112 and 95 Ma. The maximum differential stress value obtained in Well-1 is comparable to the average differential stress value (considering uncertainties) derived from calcite twins for the extensional rifting event (~45 MPa) in contrast to that obtained in Well-2 which shows a lower value. With a mean CRSS for twinning in our samples of 6–7 MPa (except for one sample from Well-2; Table 3 in Supplementary Material), this indicates that the lithostatic differential stress was likely high enough to practically cause twinning to occur under a vertical σ_1 , especially in

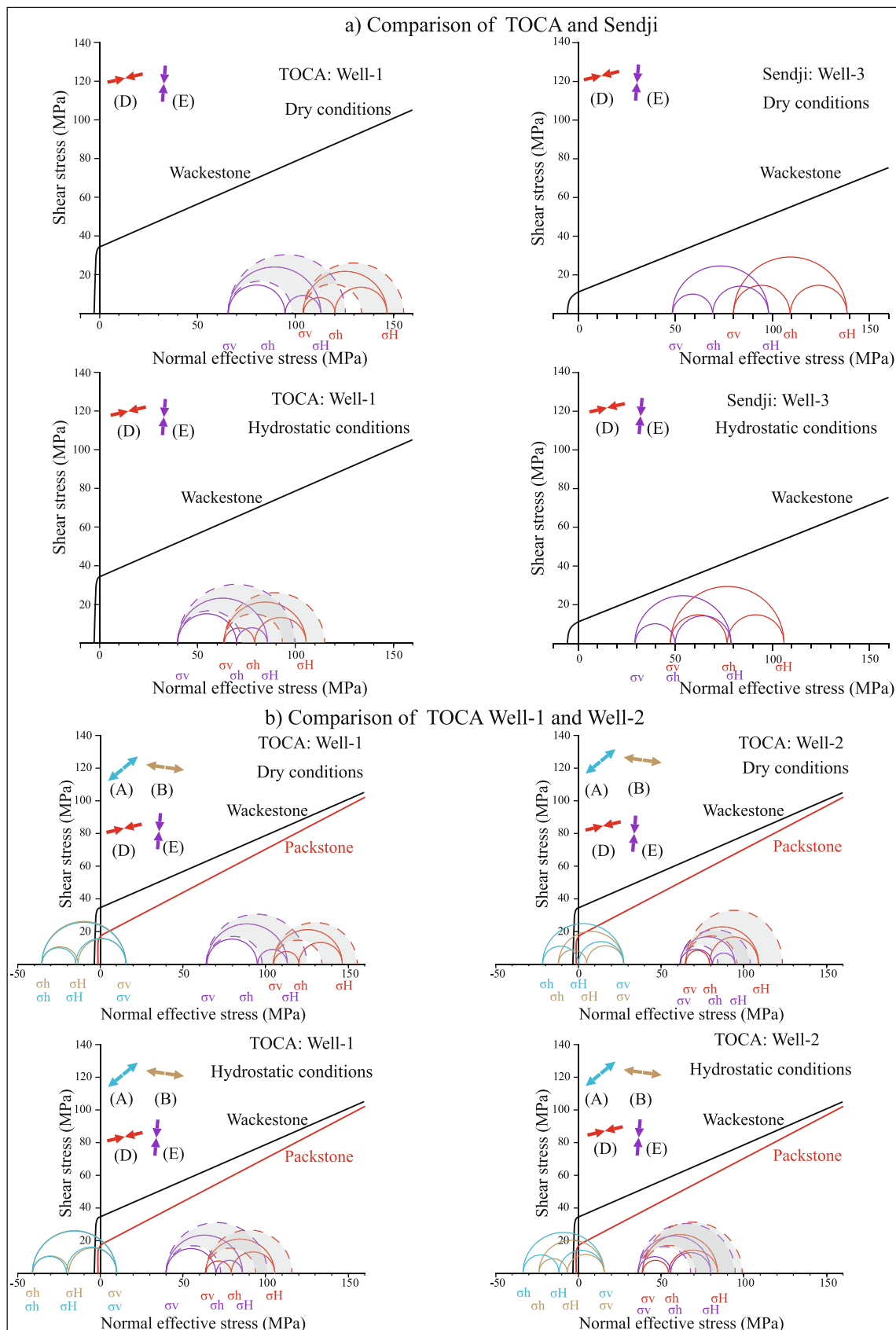


Fig. 10. Mohr diagrams displaying the failure envelope of the TOCA Fm. determined from rock mechanics tests and the Mohr circles related to the differential stress magnitudes resulting from the inversion of the calcite twins of each tectonic event, under dry and hydrostatic conditions (see text for more details). Comparison of stress magnitudes related to post-rift compressions in the TOCA and Sendji formations (a) and stress magnitudes related to syn-rift extension and post-rift compressions recorded by the TOCA Fm. in the two wells (b). The dashed circles and the greyed area in between represent the $\pm 30\%$ uncertainty on $(\sigma_1 - \sigma_3)$ values.

Well-1. Even though it is impossible to establish to what degree twinning caused by differential stress related to post-rift continuing burial may have cumulated with twinning caused by extension-related differential stress to return the high differential stress magnitudes reconstructed for the extensional stress groups, this rough estimate suggests that the burial effect might provide a reasonable explanation for the likely overestimate of extensional differential stress magnitudes (σ_1 - σ_3) using calcite twinning paleopiezometry. This still unsolved question will require further methodological and experimental developments which are out of the scope of this paper.

The absence of fit of the Mohr circles related to extensional stresses with the failure envelope (Fig. 10) precludes any definite conclusion on the occurrence of extensional mesostructures such as mode I fractures and normal faults in the studied wells. However, there is no doubt that the differential stress values related to extension were such that mode I fractures and normal faults did develop in the TOCA Fm. at regional scale (Fig. 2a).

For the stress regimes with horizontal σ_1 oriented ~N-S (stress tensor groups E) that we tentatively dated at ~67–60 Ma, the vertical stress estimated at 60 MPa is rather close for Well-1 and Well-2 (i.e., 64 MPa and 61 MPa, respectively, assuming dry conditions) (Fig. 10). The corresponding Mohr circles (Fig. 10) lie much below the rupture envelope, under both dry and hydrostatic fluid pressure conditions, and so despite uncertainties (Fig. 10). These observations indicate that the far-transferred ~N-S compressional stress was unlikely to induce fractures of either types without fluid overpressure (i.e., supra-hydrostatic fluid pressure). This is in line with the findings by Zeboudj et al. (2023) for the same compressional phase in the Sendji Fm. and with the observation that no mesostructures possibly related to ~N-S compression have been so far identified and reported from nearby wells (Fig. 10a).

For the compressional event with horizontal σ_1 oriented ~ENE-WSW (stress tensor groups D) that we tentatively dated from the middle Miocene (~15 Ma) onwards, the current vertical stress is estimated at 105 MPa and 64 MPa for Well-1 and Well-2 respectively, assuming dry conditions (Fig. 10). The corresponding Mohr circles (Fig. 10) lie much below the rupture envelope and it is the same if hydrostatic conditions are assumed. Like for the Maastrichtian-Paleocene compressional event, the differential stresses recorded for this event were unlikely to cause fractures in the TOCA Fm. Zeboudj et al. (2023) reported similar observations for the same compressional stress in the post-salt Sendji Fm (Fig. 10a).

For both compressional events, a fluid overpressure of at least 50 MPa would be needed to possibly cause fracture development. Although we cannot definitely exclude the occurrence of fluid overpressure in the TOCA reservoirs during its post-rift burial history because of the hydrocarbon migration in the Lower Congo basin from the Cenomanian to the Paleocene (Bah et al., 2023) and the occurrence of the overlying salt level that would likely act as a fluid barrier preventing upward fluid escape, the absence of any fractures consistent with the post-rift compressional events suggest that fluid overpressure -if any- never exceeded such a value.

Noticeably, the overall consistency between differential stress magnitudes recorded independently in the different wells (1 and 2) emphasizes that calcite twinning paleopiezometry is a robust and reliable method to reconstruct stress magnitude even at great depth and in complex tectonic settings.

6. Conclusions

This study focuses on the *syn*-rift, pre-salt carbonate TOCA Fm. investigated in two offshore wells in the Lower Congo basin. The novel combination of burial modelling and inversion of calcite twins for stress provides an original approach to obtain unprecedented information on the burial and paleostress history of this deeply buried reservoir. The inversion of the calcite twins allowed the determination of distinct stress regimes, the timing of which was constrained by the reconstruction of

the maximum depth of compaction-related active pressure solution combined with burial modelling.

The TOCA Fm. recorded three main tectonic events during its burial history: (1) extension between 130 and 112 Ma, with σ_3 evolving from a N100 to a NE-SW trend associated with the rifting preceding the opening of the South Atlantic; (2) intraplate ~N-S compression, possibly dated between 67 and 60 Ma and reflecting a far-field transfer of orogenic stress from the distant Africa-Eurasia active plate boundary; (3) ENE-WSW to E-W compression that we propose to mostly relate to the mid-Atlantic ridge push from ~15 Ma onwards. For each state of stress, calcite twinning paleopiezometry combined with burial modelling and rock mechanics tests enabled us to discuss the stress magnitudes which likely prevailed within the reservoir.

Our results demonstrate that the TOCA Fm. reservoir in the Lower Congo basin, and more generally the West African passive margin of the South Atlantic have recorded a complex tectonic history, including extension and compression. Beyond the reservoir scale, this study provides a new support to how tectonic and gravitational lithospheric stresses can be transferred far away from active plate boundaries and how their sequence controlled the tectonic evolution of passive margins.

CRedit authorship contribution statement

Boubacar Bah: Conceptualization, Data curation, Formal analysis, Investigation, Methodology, Writing – original draft, Writing – review & editing. **Olivier Lacombe:** Conceptualization, Formal analysis, Investigation, Writing – original draft, Writing – review & editing. **Nicolas E. Beaudoin:** Conceptualization, Investigation, Writing – original draft, Writing – review & editing. **Aniès Zeboudj:** Writing – original draft, Writing – review & editing. **Claude Gout:** Writing – original draft, Writing – review & editing. **Jean-Pierre Girard:** Writing – original draft, Writing – review & editing. **Pierre-Alexandre Teboul:** Writing – original draft, Writing – review & editing.

Declaration of Competing Interest

We have no conflict of interest to disclose.

Data availability

Data will be made available on request.

Acknowledgments

The authors are very grateful to TotalEnergies for granting financial support to this research, for providing the cores and prior data, and for permission to publish. We would like to thank Philippe Marchina for his help in carrying out the geomechanical tests and for the discussions on the results. N.E.B is funded through the isite-E2S, supported by the ANR PIA and the Région Nouvelle-Aquitaine. The authors would also like to thank the journal editor Samuel Angiboust as well as Damien Delvaux and two anonymous reviewers for their useful comments and suggestions that improved the quality of the paper.

Appendix A. Supplementary data

Supplementary data to this article can be found online at <https://doi.org/10.1016/j.tecto.2023.229997>.

References

- Affaton, P., Kalsbeek, F., Boudzoumou, F., Trompette, R., Thrane, K., Frei, R., 2016. The Pan-African West Congo belt in the Republic of Congo (Congo Brazzaville): stratigraphy of the Mayombe and West Congo Supergroups studied by detrital zircon geochronology. *Precambrian Res.* 272, 185–202.
- Al-Hajri, Y., White, N., Fishwick, S., 2009. Scales of transient convective support beneath Africa. *Geology* 37, 883–886.

- Amrouch, K., Lacombe, O., Bellahsen, N., Daniel, J.-M., Callot, J.P., 2010. Stress and strain patterns, kinematics and deformation mechanisms in a basement-cored anticline: sheep mountain anticline (Wyoming, USA). *Tectonics* 29, TC1005.
- Amrouch, K., Beaudoin, N., Lacombe, O., Bellahsen, N., Daniel, J.M., 2011. Paleostress magnitudes in folded sedimentary rocks. *Geophys. Res. Lett.* 38, L17301.
- Arboit, F., Amrouch, K., Morley, C., Collins, A.S., King, R., 2017. Palaeostress magnitudes in the Khao Khwang fold-thrust belt, new insights into the tectonic evolution of the Indosinian orogeny in Central Thailand. *Tectonophysics* 710, 266–276.
- Aslanian, D., Moulin, M., 2010. Comment on 'a new scheme for the opening of the South Atlantic Ocean and the dissection of an Aptian salt basin' by Trond H. Torsvik, Sonia Rousse, Cinthia Labails and Mark a. Smethurst. *Geophys. J. Int.* 183 (1), 20–28.
- Aslanian, D., Moulin, M., Olivet, J.L., Unternehr, P., Matias, L., Bache, F., Rabineau, M., Klingelhoefer, F., Contrucci, I., Labails, C., 2009. Brazilian and African passive margins of the Central Segment of the South Atlantic Ocean: Kinematic constraints. *Tectonophysics* 468 (1–4), 98–112.
- Asmus, H.E., Ponte, F.C., 1973. The Brazilian marginal basins. In: *The South Atlantic*. Springer, Boston, MA, pp. 87–133.
- Bah, B., Beaudoin, N.E., Lacombe, O., Girard, J.-P., Gout, C., Godeau, N., Deschamps, P., 2023. Multi-proxy reconstruction of the tectonic history and porosity evolution of the TOCA carbonate formation in the lower Congo basin (South West Africa). *Mar. Pet. Geol.* 148, 106018.
- Bate, R.H., 1999. Non-marine ostracod assemblages of the Pre-Salt rift basins of West Africa and their role in sequence stratigraphy. *Geol. Soc. Lond., Spec. Publ.* 153 (1), 283–292.
- Beaudoin, N., Lacombe, O., 2018. Recent and future trends in paleopiezometry in the diagenetic domain: insights into the tectonic paleostress and burial depth history of fold-and-thrust belts and sedimentary basins. *J. Struct. Geol.* 114, 357–365.
- Beaudoin, N., Koehn, D., Lacombe, O., Lecouty, A., Billi, A., Aharonov, E., Parlangeau, C., 2016. Fingerprinting stress: stylolite and calcite twinning paleopiezometry revealing the complexity of progressive stress patterns during folding-The case of the Monte Nero anticline in the Apennines, Italy. *Tectonics* 35, 1687–1712.
- Beaudoin, N., Lacombe, O., Koehn, D., David, M.E., Farrell, N., Healy, D., 2020. Vertical stress history and paleoburial in foreland basins unravelled by stylolite roughness paleopiezometry: Insights from bedding-parallel stylolites in the Bighorn Basin, Wyoming, USA. *J. Struct. Geol.* 136, 104061.
- Beglinger, S.E., Doust, H., Cloetingh, S., 2012. Relating petroleum system and play development to basin evolution: West African South Atlantic basins. *Mar. Pet. Geol.* 30 (1), 1–25.
- Bidiet, J., Kinga, A., Loemba, C., Assoua-Wande, C., Hossie, G., Mahoukou-Sounga, A., 1998. Aperçu géologique et pétrolier des bassins du Congo. Rapport de l'association des producteurs de pétrole africains. In: *Hydro-Congo, Elf-Congo, AGIP Congo*, Ministère des Mines et de l'Énergie. RF11904.
- Bjørlykke, K., 2014. Relationships between depositional environments, burial history and rock properties. Some principal aspects of diagenetic process in sedimentary basins. *Sediment. Geol.* 301, 1–14.
- Bott, M.H.P., 1993. Modelling the plate-driving mechanism. *J. Geol. Soc.* 150 (5), 941–951.
- Brandstätter, J., Kurz, W., Rogowitz, A., 2017. Microstructural analysis and calcite piezometry on hydrothermal veins: Insights into the deformation history of the Cocos Plate at Site U1414 (IODP Expedition 344). *Tectonics* 36 (8), 1562–1579.
- Braun, J., Guillocheau, F., Robin, C., Baby, G., Jelsma, H., 2014. Eroding a large continental area by tilting it over a source of mantle upwelling to explain the late cretaceous south African erosional event. *Geophys. Res. Abstr.* 16 (EGU2014–4219).
- Brice, S.E., Cochran, M.D., Pardo, G., Edwards, A.D., 1982. Tectonics and sedimentation of the South Atlantic rift sequence: Cabinda, Angola: rifted margins: field investigations of margin structure and stratigraphy. In: *Studies in Continental Margin Geology*, AAPG Special Volumes, pp. 5–18.
- Brognon, G.P., Verrier, G.R., 1966. Oil and geology in Cuanza Basin of Angola. *AAPG Bull.* 50 (1), 108–158.
- Brownfield, M.E., Charpentier, R.R., 2006. Geology and total petroleum systems of the West-Central Coastal Province (7203), West Africa. *U. S. Geol. Surv. Bull.* 2207-B, 52.
- Bullard, E.C., 1965. Fit of the continents around the Atlantic. *Science* 148, 664.
- Burkhard, M., 1993. Calcite twins, their geometry, appearance and significance as stress-strain markers and indicators of tectonic regime: a review. *J. Struct. Geol.* 15 (3–5), 351–368.
- Burov, E., Gerya, T., 2014. Asymmetric three-dimensional topography over mantle plumes. *Nature* 513 (7516), 85–89.
- Burwood, R., 1999. Angola: source rock control for lower Congo Coastal and Kwanza Basin petroleum systems. *Geol. Soc. Lond., Spec. Publ.* 153 (1), 181–194.
- Carminatti, M., Wolff, B., Gamboa, L., 2008. New Exploratory Frontiers in Brazil. In: *Proceedings of the 19th World Petroleum Congress*. Spain, Madrid. June 29–July 3, 2008, p. 11.
- Chaboureaud, A.C., Guillocheau, F., Robin, C., Rohais, S., Moulin, M., Aslanian, D., 2013. Paleogeographic evolution of the central segment of the South Atlantic during early cretaceous times: Paleotopographic and geodynamic implications. *Tectonophysics* 604, 191–223.
- Cloetingh, S., Burov, E., Matenco, L., Beekman, F., Roue, F., Ziegler, P.A., 2013. The Moho in extensional tectonic settings: Insights from thermo-mechanical models. *Tectonophysics* 609, 558–604.
- Cobbold, P.R., Meisling, K.E., Mount, V.S., 2001. Reactivation of an obliquely rifted margin, Campos and Santos basins, southeastern Brazil. *AAPG Bull.* 85, 1925–1944.
- Contrucci, I., Matias, L., Moulin, M., Géli, L., Klingelhoefer, F., Nouzé, H., Aslanian, D., Olivet, J.L., Réhault, J.P., Sibuet, J.C., 2004. Deep structure of the West African continental margin (Congo, Zaire, Angola), between 5°S and 8°S, from reflection/refraction seismics and gravity data. *Geophys. J. Int.* 158 (2), 529–553.
- Craddock, J.P., Jackson, M., van der Pluijm, B.A., Versical, R.T., 1993. Regional shortening fabrics in eastern North America: Far-field stress transmission from the Appalachian-Ouachita Orogenic Belt. *Tectonics* 12 (1), 257–264.
- Craddock, J.P., Farris, D.W., Roberson, A., 2004. Calcite-twinning constraints on stress-strain fields along the Mid-Atlantic Ridge, Iceland. *Geology* 32 (1), 49–52.
- Craddock, J.P., Pearson, A.M., 1994. Non-coaxial horizontal shortening strains preserved in twinned amygdule calcite, DSDP Hole 433, Suiko seamount, northwest Pacific plate. *J. Struct. Geol.* 16 (5), 719–724.
- Da Costa, J.L., Schirmer, T.W., Laws, B.R., 1999. Lower Congo basin, Deepwater exploration province, offshore West Africa. *AAPG Bull.* 83 (12).
- Dale, C.T., Lopes, J.R., Abilio, S., 1992. Takula oil field and the Greater Takula area, Cabinda, Angola. In: Halbouty, M.T. (Ed.), *Giant Oil and Gas Fields of the Decade 1978–1988*, 54. AAPG Memoir, pp. 197–215.
- Daly, M.C., Lawrence, S.R., Diemu-Tshiband, K., Matouana, B., 1992. Tectonic evolution of the cuvette Centrale, Zaire. *J. Geol. Soc.* 149 (4), 539–546.
- Dauteuil, O., Deschamps, F., Bourgeois, O., Mocquet, A., Guillocheau, F., 2013. Post-breakup evolution and paleotopography of the North Namibian margin during the Meso-Cenozoic. *Tectonophysics* 589, 103–115.
- Davison, I., 2007. Geology and tectonics of the South Atlantic Brazilian salt basins. *Geol. Soc. Lond., Spec. Publ.* 272 (1), 345–359.
- De Bresser, J.H.P., Spiers, C.J., 1997. Strength characteristics of the r, f, and c slip systems in calcite. *Tectonophysics* 272, 1–23.
- Delpomdor, F., Tack, L., Prétat, A., 2008. Microstructures in the Neoproterozoic tillites around the Congo River Basin (CRB), Democratic Republic of Congo (DRC): Comparison with the Karoo tillites from the Dekese borehole in the CRB. In: *22nd Colloquium of African Geology (CAG22) & 13th Conference of the Geological Society of Africa (GSAf13)*, p. 108.
- Delvaux, D., Barth, A., 2010. African stress pattern from formal inversion of focal mechanism data. *Tectonophysics* 482 (1–4), 105–128.
- Delvaux, D., Maddaloni, F., Tesauro, M., Braitenberg, C., 2021. The Congo Basin: Stratigraphy and subsurface structure defined by regional seismic reflection, refraction and well data. *Glob. Planet. Chang.* 198 (2), 103407.
- Dingle, R.V., 1999. Walvis Ridge barrier: its influence on palaeoenvironments and source rock generation deduced from ostracod distributions in the early South Atlantic Ocean. *Geol. Soc. Lond., Spec. Publ.* 153 (1), 293–302.
- Doyle, J.A., Jardine, S., Doerenkamp, A., 1982. Afropolis, un nouveau genre de pollen d'Angiosperme précoce, avec de données sur la palynostratigraphie et les paléoenvironnements du Crétacé du Nord-Gondwana. *Bull. Centres Recherche d'Explorat.-Product. Elf-Aquitaine* 6, 39–117.
- Etchecopar, A., 1984. Etudes des états de contrainte en tectonique cassante et simulations de déformations plastiques (approche mathématiques). Unpublished thesis. Université des Sciences et Techniques du Languedoc.
- Fernandes, A.J., Amaral, G., 2002. Cenozoic tectonic events at the border of the Paraná Basin, São Paulo, Brazil. *J. S. Am. Earth Sci.* 14, 911–931.
- Ferrari, A.L., 2001. Evolução Tectônica do Graben da Guanabara (PhD thesis). Instituto de Geociências da Universidade de São Paulo, p. 412.
- Ferrill, D.A., 1998. Critical re-evaluation of differential stress estimates from calcite twins in coarse-grained limestone. *Tectonophysics* 285, 77–86.
- Ferrill, D.A., Morris, A.P., Evans, M.A., Burkhard, M., Groshong Jr., R.H., Onasch, C.M., 2004. Calcite twin morphology: a low-temperature deformation geothermometer. *J. Struct. Geol.* 26 (8), 1521–1529.
- Flament, N., Gurnis, M., Williams, S., Seton, M., Skogseid, J., Heine, C., Müller, R.D., 2014. Topographic asymmetry of the South Atlantic from global models of mantle flow and lithospheric stretching. *Earth Planet. Sci. Lett.* 387, 107–119.
- Giresse, P., 1982. La succession des sédiments dans les bassins marins et continentaux du Congo depuis le début du Mésozoïque. *Sci. Géol., Bull. Mémoire.* 35 (4), 183–206.
- Goscombe, B.D., Gray, D.R., 2008. Structure and strain variation at mid-crustal levels in a transpressional orogen: a review of Kaoko Belt structure and the character of West Gondwana amalgamation and dispersal. *Gondwana Res.* 13, 45–85.
- Gradstein, F.M., Ogg, J.G., Smith, A.G., Bleeker, W., Lourens, L.J., 2004. A new geologic time scale, with special reference to Precambrian and Neogene. *Episodes* 27 (2), 83–100.
- Grosdidier, E., 1967. Quelques ostracodes nouveaux de la Série anté-salifère ("Wealdienne") des bassins côtiers du Gabon et du Congo. *Rev. Micropaleontol.* 10 (2), 107–118.
- Grosdidier, E., Braccini, E., Dupont, G., Moron, J.M., 1996. Biozonation du Crétacé Inférieur non marin des bassins du Gabon et du Congo. *Bulletin des Centres de recherches exploration-production Elf-Aquitaine. Memoir* 16, 67–82.
- Guardado, L.R., Gamboa, L.A.P., Lucchesi, C.F., 1989. Petroleum Geology of the Campos Basin, Brazil, A Model for a Producing Atlantic Type Basin: Part 1.
- Guiraud, R., Bosworth, W., 1997. Senonian basin inversion and rejuvenation of rifting in Africa and Arabia: synthesis and implications to plate-scale tectonics. *Tectonophysics* 282 (1–4), 39–82.
- Guiraud, R., Maurin, J.C., 1991. Le Rifting en Afrique au Cretace inferieur; synthese structurale, mise en evidence de deux etapes dans la genese des bassins, relations avec les ouvertures oceaniques peri-africaines. *Bull. Soc. Géol. France* 162 (5), 811–823.
- Guiraud, M., Buta-Neto, A., Quesne, D., 2010. Segmentation and differential post-rift uplift at the Angola margin as recorded by the transform-rifted Benguela and oblique-to-orthogonal-rifted Kwanza basins. *Mar. Pet. Geol.* 27 (5), 1040–1068.
- Harris, N.B., 2000. TOCA Carbonate, Congo Basin: response to an evolving rift lake. In: Mello, M.R., Katz, B.J. (Eds.), *Petroleum Systems of South Atlantic Margins: American Association of Petroleum Geologists Memoir*, 73, pp. 341–360.

- Heidbach, O., Reinecker, J., Tingay, M., Müller, B., Sperner, B., Fuchs, K., Wenzel, F., 2007. Plate boundary forces are not enough: Second- and third-order stress patterns highlighted in the World Stress Map database. *Tectonics* 26, TC6014.
- Heidbach, O., Tingay, M., Barth, A., Reinecker, J., Kurfess, D., Müller, B., 2008. The 2008 release of the World Stress Map. available online at www.world-stress-map.org.
- Heidbach, O., Rajabi, M., Reiter, K., Ziegler, M., 2016. World Stress Map 2016. GFZ Data Services.
- Heine, C., Zoethout, J., Müller, R.D., 2013. Kinematics of the South Atlantic rift. *Solid Earth* 5 (1), 41–116.
- Hu, J.C., Angelier, J., 2004. Stress permutations: Three-dimensional distinct element analysis accounts for a common phenomenon in brittle tectonics. *J. Geophys. Res. Solid Earth* 109 (B9).
- Jamison, W.R., Spang, J.H., 1976. Use of calcite twin lamellae to infer differential stress. *Geol. Soc. Am. Bull.* 87 (6), 868–872.
- Japsen, P., Chalmers, J.A., Green, P.F., Bonow, J.M., 2012. Elevated, passive continental margins: not rift shoulders, but expressions of episodic, post-rift burial and exhumation. *Glob. Planet. Chang.* 90–91, 73–86.
- Johnston, S.T., 2000. The Cape Fold Belt and Syntaxis and the rotated Falkland Islands: dextral transpressional tectonics along the southwest margin of Gondwana. *J. Afr. Earth Sci.* 31 (1), 51–63.
- Jolivet, L., Baudin, T., Calassou, S., Chevrot, S., Ford, M., Issautier, B., Lasseur, E., Masini, E., Manatschal, G., Mouthereau, F., Thion, I., Vidal, O., 2021. Geodynamic evolution of a wide plate boundary in the Western Mediterranean, near-field versus far-field interactions. *BSGF-Earth Sci. Bull.* 192 (1), 48.
- Kadima, E., Delvaux, D., Sebagenzi, S.N., Tack, L., Kabeya, S.M., 2011. Structure and geological history of the Congo Basin: an integrated interpretation of gravity, magnetic and reflection seismic data. *Basin Res.* 23 (5), 499–527.
- Karl, M., Glasmacher, U.A., Kollenz, S., Franco-Magalhaes, A.O.B., Stockli, D.F., Hacksbacher, P.C., 2013. Evolution of the South Atlantic passive continental margin in southern Brazil derived from zircon and apatite (U–Th–Sm)/he and fission-track data. *Tectonophysics* 604, 224–244.
- Karner, G.D., Driscoll, N.W., 1999. Tectonic and stratigraphic development of the West African and eastern Brazilian margins: insights from quantitative basin modelling. *Geol. Soc. Lond., Spec. Publ.* 153 (1), 11–40.
- Karner, G.D., Gambôa, L.A.P., 2007. Timing and origin of the South Atlantic pre-salt sag basins and their capping evaporites. *Geol. Soc. Lond., Spec. Publ.* 285 (1), 15–35.
- Karner, G.D., Driscoll, N.W., McGinnis, J.P., Brumbaugh, W.D., Cameron, N.R., 1997. Tectonic significance of syn-rift sediment packages across the Gabon-Cabinda continental margin. *Mar. Pet. Geol.* 14 (7), 973–1000.
- Karner, G.D., Driscoll, N.W., Barker, D.H.N., 2003. Syn-rift regional subsidence across the West African continental margin: the role of lower plate ductile extension. *Geol. Soc. Lond., Spec. Publ.* 207 (1), 105–129.
- Koptev, A., Burrov, E., Gerya, T., Le Pourhiet, L., Leroy, S., Calais, E., Jolivet, L., 2018. Plume-induced continental rifting and break-up in ultra-slow extension context: Insights from 3D numerical modeling. *Tectonophysics* 746, 121–137.
- Kounov, A., Viola, G., De Wit, M., Andreoli, M.A.G., 2009. Denudation along the Atlantic passive margin: new insights from apatite fission-track analysis on the western coast of South Africa. *Geol. Soc. Lond., Spec. Publ.* 324 (1), 287–306.
- Kulikowski, D., Amrouch, K., 2017. Combining geophysical data and calcite twin stress inversion to refine the tectonic history of subsurface and offshore provinces: a case study on the Cooper-Eromanga Basin, Australia. *Tectonics* 36 (3), 515–541.
- Labeur, A., Beaudoin, N.E., Lacombe, O., Emmanuel, L., Petracchini, L., Daëron, M., Klimowicz, S., Callot, J.P., 2021. Burial-deformation history of folded rocks unraveled by fracture analysis, stylolite paleopiezometry and vein cement geochemistry: a case study in the Cingoli Anticline (Umbria-Marche, Northern Apennines). *Geosciences* 11 (3), 135.
- Lacombe, O., 2001. Paleostress magnitudes associated with development of mountain belts: insights from tectonic analyses of calcite twins in the Taiwan Foothills. *Tectonics* 20 (6), 834–849.
- Lacombe, O., 2007. Comparison of paleostress magnitudes from calcite twins with contemporary stress magnitudes and frictional sliding criteria in the continental crust: Mechanical implications. *J. Struct. Geol.* 29 (1), 86–99.
- Lacombe, O., 2010. Calcite twins, a tool for tectonic studies in thrust belts and stable orogenic forelands. *Oil & Gas Sci. Technol.—Revue d'IFP Energ. Nouvell.* 65 (6), 809–838.
- Lacombe, O., Laurent, P., 1992. Determination of principal stress magnitudes using calcite twins and rock mechanics data. *Tectonophysics* 202, 83–93.
- Lacombe, O., Laurent, P., 1996. Determination of deviatoric stress tensors based on inversion of calcite twin data from experimentally deformed monophase samples: preliminary results. *Tectonophysics* 255 (3–4), 189–202.
- Lacombe, O., Angelier, J., Laurent, P., Bergerat, F., Tournier, C., 1990. Joint analyses of calcite twins and fault slips as a key for deciphering polyphase tectonics: Burgundy as a case study. *Tectonophysics* 182 (3–4), 279–300.
- Lacombe, O., Laurent, P., Angelier, J., Roure, F., 1994. Calcite twins as a key to paleostresses in sedimentary basins: Preliminary results from drill cores of the Paris basin. *Peri-Tethyan Platforms* 197–210.
- Lacombe, O., Amrouch, K., Mouthereau, F., Dissez, L., 2007. Calcite twinning constraints on late Neogene stress patterns and deformation mechanisms in the active Zagros collision belt. *Geology* 35 (3), 263–266.
- Lacombe, O., Malandain, J., Vilasi, N., Amrouch, K., Roure, F., 2009. From paleostresses to paleoburial in fold-thrust belts: preliminary results from calcite twin analysis in the outer Albanides. *Tectonophysics* 475, 128–141.
- Lacombe, O., Parlangeau, C., Beaudoin, N.E., Amrouch, K., 2021a. Calcite Twin Formation, Measurement and Use as Stress-Strain Indicators: A Review of Progress over the Last Decade. *Geosciences* 11 (11), 445.
- Lacombe, O., Beaudoin, N., Hoareau, G., Labeur, A., Pecheyran, C., Callot, J.P., 2021b. Dating folding beyond folding, from layer-parallel shortening to fold tightening, using mesostructures: Lessons from the Apennines, Pyrenees and rocky mountains. *Solid Earth* 12 (10), 2145–2157.
- Laurent, P., Bernard, P., Vasseur, G., Etchecopar, A., 1981. Stress tensor determination from the study of e twins in calcite: a linear programming method. *Tectonophysics* 78 (1–4), 651–660.
- Laurent, P., Kern, H., Lacombe, O., 2000. Determination of deviatoric stress tensors based on inversion of calcite twin data from experimentally deformed monophase samples. Part II. Axial and triaxial stress experiments. *Tectonophysics* 327 (1–2), 131–148.
- Lehner, P., De Ruiter, P.A.C., 1977. Structural history of the Atlantic margin of Africa. *AAPG Bull.* 61 (7), 961–981.
- Lima, C., Nascimento, E., Assumpção, M., 1997. Stress orientations in Brazilian sedimentary basins from breakout analysis: implications for force models in the south American plate. *Geophys. J. Int.* 130, 112–124.
- Loparev, A., Rouby, D., Chardon, D., Dall'Asta, M., Sapin, F., Bajeot, F., Ye, J., Paquet, F., 2021. Superimposed rifting at the junction of the Central and Equatorial Atlantic: formation of the passive margin of the Guiana Shield. *Tectonics* 40 (7) e2020TC006159.
- Machado, R., Roldan, L.F., Jacques, P.D., Fassbinder, E., Nummer, A.R., 2012. Tectónica transcorrente Mesozoica-Cenozoica no Domo de Lages-Santa Catarina. *Rev. Bras. Geosci.* 42, 799–811.
- Mahatsente, R., Coblent, D., 2015. Ridge-push force and the state of stress in the Nubia-Somalia plate system. *Lithosphere* 7 (5), 503–510.
- Marton, L.G., Tari, G.C., Lehmann, C.T., Mohriak, W., 2000. Evolution of the Angolan passive margin, West Africa, with emphasis on post-salt structural styles. *Geophys. Monograph-American Geophysical Union.* 115, 129–150.
- Masson, M.P., 1972. L'exploration pétrolière en Angola. *Rev. de l'Assoc. Franç. Techn. Pétrole* v, 212.
- Matton, G., Jébrak, M., 2009. The cretaceous Peri-Atlantic Alkaline Pulse (PAAP): deep mantle plume origin or shallow lithospheric break-up? *Tectonophysics* 469 (1–4), 1–12.
- Mbina Mounquengui, M., Guiraud, M., 2009. Neocomian to early Aptian syn-rift evolution of the normal to oblique-rifted North Gabon margin (interior and N'Komi basins). *Mar. Pet. Geol.* 26 (6), 1000–1017.
- McHargue, T.R., 1990. Stratigraphic Development of Proto-South Atlantic Rifting in Cabinda, Angola—A Petroliferous Lake Basin: Chapter 19.
- Medvedev, S., 2016. Understanding lithospheric stresses: systematic analysis of controlling mechanisms with applications to the African Plate. *Geophys. J. Int.* 207 (1), 393–413.
- Mohriak, W., Nemčok, M., Enciso, G., 2008. South Atlantic divergent margin evolution: rift-border uplift and salt tectonics in the basins of SE Brazil. *Geol. Soc. Lond., Spec. Publ.* 294 (1), 365–398.
- Morley, C.K., Gabdi, S., Seesuthi, K., 2007. Fault superimposition and linkage resulting from stress changes during rifting: examples from 3D seismic data, Phitsanulok Basin, Thailand. *J. Struct. Geol.* 29 (4), 646–663.
- Moucha, R., Forte, A.M., 2011. Changes in African topography driven by mantle convection. *Nat. Geosci.* 4, 707–712.
- Moulin, M., Aslanian, D., Olivet, J.L., Contrucci, I., Matias, L., Géli, L., Klingelhoefer, F., Nouzé, H., Untermeir, P., 2005. Geological constraints on the evolution of the Angolan margin based on reflection and refraction seismic data (ZaiAngo project). *Geophys. J. Int.* 162 (3), 793–810.
- Moulin, M., Aslanian, D., Untermeir, P., 2010. A new starting point for the South and Equatorial Atlantic Ocean. *Earth Sci. Rev.* 98 (1–2), 1–37.
- Muller, R.D., Seton, M., Zahirovic, S., Williams, S.E., Matthews, K.J., Wright, N.M., Shephard, G.E., Maloney, K.T., Barnett-Moore, N., Hosseinpour, M., Bower, D.J., Cannon, J., 2016. Ocean basin evolution and global-scale plate reorganization events since Pangea breakup. *Annu. Rev. Earth Planet. Sci.* 44 (1), 107–138.
- Mussard, J.M., 1996. Les palynomorphes, indicateurs des variations du niveau marin relatif: analyses quantitatives dans l'Albien supérieur de la République du Congo. In: Jardine, S., de Klaz, I., Debenay, J.-P. (Eds.), *Géologie de l'Afrique et de l'Atlantique Sud, Compte Rendus des Colloques de géologie d'Angers, 16–24 juillet 1994*, 16. Mémoires du Bulletin des Centres de Recherche et d'Exploration-Production d'Elf, pp. 57–66.
- Nkodia, H.V., Miyouna, T., Delvaux, D., Boudzoumou, F., 2020. Flower structures in sandstones of the Paleozoic Inkisi Group (Brazzaville, Republic of Congo): evidence for two major strike-slip fault systems and geodynamic implications. *S. Afr. J. Geol.* 123 (4), 531–550.
- Nkodia, H.M.D.-V., Miyouna, T., Kolawole, F., Boudzoumou, F., Loemba, A.P.R., Babezibonza Tchiguina, N.C., Delvaux, D., 2022. Seismogenic fault reactivation in western Central Africa: Insights from regional stress analysis. *Geochem. Geophys. Geosyst.* 23 e2022GC010377.
- Nurnberg, D., Müller, R.D., 1991. The tectonic evolution of the South Atlantic from late Jurassic to present. *Tectonophysics* 191 (1–2), 27–53.
- Parlangeau, C., Lacombe, O., Schueller, S., Daniel, J.M., 2018. Inversion of calcite twin data for paleostress orientations and magnitudes: a new technique tested and calibrated on numerically-generated and natural data. *Tectonophysics* 722, 462–485.
- Parlangeau, C., Dimanov, A., Lacombe, O., Hallais, S., Daniel, J.M., 2019. Uniaxial compression of calcite single crystals at room temperature: insights into twinning activation and development. *Solid Earth* 10 (1), 307–316.
- Pascal, C., 2006. On the role of heat flow, lithosphere thickness and lithosphere density on gravitational potential stresses. *Tectonophysics* 425, 83–99.

- Pascal, C., Cloetingh, S.A., 2009. Gravitational potential stresses and stress field of passive continental margins: Insights from the South-Norway shelf. *Earth Planet. Sci. Lett.* 277 (3–4), 464–473.
- Passchier, C.W., Trouw, R.A.J., Ribeiro, A., Pacifullo, F.V.P., 2002. Tectonic evolution of the southern Kaoko belt, Namibia. *J. Afr. Earth Sci.* 35, 61–75.
- Pedrosa-Soares, A.C., Noce, C.M., Vidal, P., Monteiro, R.L.B.P., Leonardos, O.H., 1992. Toward a new tectonic model for the late proterozoic Araçuaí (SE Brazil)–West Congolian (SW Africa) belt. *J. S. Am. Earth Sci.* 6 (1–2), 33–47.
- Pérez-Díaz, L., Eagles, G., 2014. Constraining South Atlantic growth with seafloor spreading data. *Tectonics* 33, 1848–1873.
- Péron-Pinvidic, G., Manatschal, G., Masini, E., Sutra, E., Flament, J.M., Hauptert, I., Unternehr, P., 2017. Unravelling the along-strike variability of the Angola–Gabon rifted margin: a mapping approach. *Geological Society, London, Special Publications* 438 (1), 49–76.
- Pletsch, T., Erbacher, J., Holbourn, A.E., Kuhnt, W., Moullade, M., Obob-Ikuenobede, F. E., Söding, E., Wagner, T., 2001. Cretaceous separation of Africa and South America: the view from the West African margin (ODP Leg 159). *J. S. Am. Earth Sci.* 14 (2), 147–174.
- Préat, A., Kolo, K., Prian, J.P., Delpomdor, F., 2010. A peritidal evaporite environment in the Neoproterozoic of South Gabon (Schisto-Calcaire Subgroup, Nyanga Basin). *Precambrian Res.* 177 (3–4), 253–265.
- Rabinowitz, P.D., LaBrecque, J., 1979. The Mesozoic South Atlantic Ocean and evolution of its continental margins. *J. Geophys. Res. Solid Earth* 84 (B11), 5973–6002.
- Reis, Á.F.C., Bezerra, F.H.R., Ferreira, J.M., do Nascimento, A.F., Lima, C.C., 2013. Stress magnitude and orientation in the Potiguar Basin, Brazil: implications on faulting style and reactivation. *J. Geophys. Res. Solid Earth* 118.
- Riccomini, C., 1995. Padrão de fraturamentos do Maciço Alcalino de Cananéia, Estado de São Paulo: relações com a tectônica mesozóico-cenozóica do sudeste do Brasil. *Rev. Bras. Geosci.* 25, 79–84.
- Ritsema, J., Deuss, A., van Heijst, H.J., Woodhouse, J.H., 2011. S40RTS: a degree-40 shear velocity model for the mantle from new Rayleigh wave dispersion, teleseismic traveltimes and normal-mode splitting function measurements. *Geophys. J. Int.* 184, 1223–1236.
- Rocher, M., Lacombe, O., Angelier, J., Chen, H.-W., 1996. Mechanical twin sets in calcite as markers of recent collisional events in a fold-and-thrust belt: evidence from the reefal limestones of southwestern Taiwan. *Tectonics* 15 (5), 984–996.
- Rocher, M., Lacombe, O., Angelier, J., Deffontaines, B., Verdier, F., 2000. Cenozoic folding and faulting in the North Pyrenean Foreland (Aquitaine Basin, France): insights from combined structural and paleostress analyses. *J. Struct. Geol.* 22 (5), 627–645.
- Rocher, M., Cushing, M., Lemeille, F., Lozac'h, Y., Angelier, J., 2004. Intraplate paleostresses reconstructed with calcite twinning and faulting: improved method and application to the eastern Paris Basin (Lorraine, France). *Tectonophysics* 387, 1–21.
- Rowe, K.J., Rutter, E.H., 1990. Palaeostress estimation using calcite twinning: experimental calibration and application to nature. *J. Struct. Geol.* 12, 1–17.
- Saller, A., Rushton, S., Buambua, L., Inman, K., McNeil, R., Dickson, J.A.D., 2016. Presalt stratigraphy and depositional systems in the Kwanza Basin, offshore Angola. *AAPG Bull.* 100 (7), 1135–1164.
- Salomon, E., Koehn, D., Passchier, C., Hackspacher, P.C., Glasmacher, U.A., 2015. Contrasting stress fields on correlating margins of the South Atlantic. *Gondwana Res.* 28 (3), 1152–1167.
- Schoellkopf, N.B., Patterson, B.A., 2000. Petroleum systems of offshore, Cabinda, Angola. In: Mello, M.R., Katz, B.J. (Eds.), *Petroleum systems of South Atlantic margins*, 73. AAPG Memoir, pp. 361–376.
- Seeber, L., Armbruster, J.G., 1988. Seismicity along the Atlantic Seaboard of the US; Intraplate neotectonics and earthquake hazards. The Atlantic continental margin, US: Boulder, Colorado, Geological Society of America. *Geol. N. Am.* I-2, 565–582.
- Séranne, M., Anka, Z., 2005. South Atlantic continental margins of Africa: a comparison of the tectonic vs climate interplay on the evolution of equatorial West Africa and SW Africa margins. *J. Afr. Earth Sci.* 43 (1–3), 283–300.
- Standlee, L., Brumbaugh, W., Cameron, N., 1992. Controlling factors in the initiation of the South Atlantic rift system. *Compte rendus des colloques de géologie de Libreville, Elf Aquitaine. Mémoire Elf Aquitaine* 13.
- Stein, C.A., Cloetingh, S., R., 1989. Wortel, Seasat-derived gravity constraints on stress and deformation in the northeastern Indian Ocean. *Geophys. Res. Lett.* 16, 823–826.
- Szatmari, P., Milani, E.J., 2016. Tectonic control of the oil-rich large igneous-carbonate-salt province of the South Atlantic rift. *Mar. Pet. Geol.* 77, 567–596.
- Tack, L., Wingate, M.T.D., Liegeois, J.-P., Fernandez-Alonso, M., Deblond, A., 2001. Early Neoproterozoic magmatism (1000–910Ma) of the Zadinian and Mayumbian groups (Bas-Congo): onset of Rodinia rifting at the western edge of the Congo craton. *Precambrian Res.* 110, 277–306.
- Teboul, P.-A., 2017. Diagenesis of Lower Cretaceous Presalt Continental Carbonates from the West African Margin Simulations and Analogues. Unpublished thesis. Aix-Marseille Université.
- Teisserenc, P., Villemin, J., 1989. Sedimentary basin of Gabon—geology and oil systems. In: Edwards, J.D., Santogrossi, P.A. (Eds.), *Divergent/Passive Margins Basins*, 48 (1990). AAPG, pp. 117–199.
- Thompson, D.L., Stiiwell, J.D., Hall, M., 2015. Lacustrine carbonate reservoirs from early cretaceous rift lakes of Western Gondwana: Pre-salt coquinas of Brazil and West Africa. *Gondwana Res.* 28 (1), 26–51.
- Torsvik, T.H., Rousse, S., Labails, C., Smethurst, M.A., 2009a. A new scheme for the opening of the South Atlantic Ocean and the dissection of an Aptian salt basin. *Geophys. J. Int.* 177, 1315–1333.
- Torsvik, T.H., Rousse, S., Labails, C., Smethurst, M.A., 2009b. A new scheme for the opening of the South Atlantic Ocean and the dissection of an Aptian salt basin. *Geophys. J. Int.* 177 (3), 1315–1333.
- Tourmeret, C., Laurent, P., 1990. Paleo-stress orientations from calcite twins in the North Pyrenean foreland, determined by the Etchecopar inverse method. *Tectonophysics* 180 (2–4), 287–302.
- Tullis, T.E., 1980. The use of mechanical twinning in minerals as a measure of shear stress magnitudes. *J. Geophys. Res. Solid Earth* 85 (B11), 6263–6268.
- Turner, F.J., 1953. Nature and dynamic interpretation of deformation lamellae in calcite of three marbles. *Am. J. Sci.* 251, 276–298.
- Turner, F.J., Griggs, D.T., Heard, H., 1954. Experimental deformation of calcite crystals. *Geol. Soc. Am. Bull.* 65 (9), 883–934.
- Uncini, G., Brandao, M., Giovannelli, A., 1998. Neocomian–Upper Aptian Pre-Salt sequence of southern Kwanza Basin: A regional view. In: ABGP/AAPG International Conference and Exhibition November 8–11, 1998, Rio de Janeiro, Brazil.
- Vagnes, E., Gabrielsen, R.H., Haremo, P., 1998. Late Cretaceous–Cenozoic intraplate contractional deformation at the Norwegian continental shelf: timing, magnitude and regional implications. *Tectonophysics* 300 (1–4), 29–46.
- Vernet, R., Assoua-Wande, C., Massamba, L., Sorriaux, P., 1996. Paléogéographie du Crétacé (Albien–Maastrichtien) du bassin côtier congolais. *Bull. Cent. Recherch. Explorat.-Product. Elf-Aquitaine Mémoire* 16, 39–55.
- Vink, G.R., 1982. Continental rifting and the implication for plate tectonics reconstructions. *J. Geophys. Res.* 87, 10677–10688.
- Viola, G., Andreoli, M., Ben-Avraham, Z., Stengel, I., Reshef, M., 2005. Offshore mud volcanoes and onland faulting in southwestern Africa: neotectonic implications and constraints on the regional stress field. *Earth Planet. Sci. Lett.* 231, 147–160.
- Viola, G., Kounov, A., Andreoli, M.A.G., Mattila, J., 2012. Brittle tectonic evolution along the western margin of South Africa: more than 500 Myr of continued reactivation. *Tectonophysics* 514, 93–114.
- Wakamori, K., Yamaji, A., 2020. The integrated stress-strain analysis of calcite twins: Consistent stress and strain determined from natural data. In: EGU General Assembly Conference Abstracts. European Geosciences Union, Vienna, p. 12819.
- Wiens, D.A., Stein, S., 1983. Age dependence of oceanic intraplate seismicity and implications for lithospheric evolution. *J. Geophys. Res. Solid Earth* 88 (B8), 6455–6468.
- Wiens, D.A., Stein, S., 1985. Implications of oceanic intraplate seismicity for plate stresses, driving forces and rheology. *Tectonophysics* 116 (1–2), 143–162.
- Withjack, M.O., Olsen, P.E., Schlische, R.W., 1995. Tectonic evolution of the Fundy rift basin, Canada: evidence of extension and shortening during passive margin development. *Tectonics* 14 (2), 390–405.
- Yamaji, A., 2015. Generalized Hough transform for the stress inversion of calcite twin data. *J. Struct. Geol.* 80, 2–15.
- Zeboudj, A., Bah, B., Lacombe, O., Beaudoin, N.E., Gout, C., Godeau, N., Girard, J.-P., Deschamps, P., 2023. Depicting past stress history at passive margins: a combination of calcite twinning and stylolite roughness paleopiezometry in supra-salt Sendji deep carbonates, lower Congo Basin, West Africa. *Mar. Pet. Geol.* 152, 106219.
- Ziegler, P.A., Cloetingh, S., van Wees, J.D., 1995. Dynamics of intra-plate compressional deformation: the Alpine foreland and other examples. *Tectonophysics* 252 (1–4), 7–59.
- Zoback, M.L., 1992. First-and second-order patterns of stress in the lithosphere: the World stress Map Project. *J. Geophys. Res. Solid Earth* 97 (B8), 11703–11728.